Graphical Abstract

Analytical Vibration Modelling and Solution of Bars with Frictional Clamps

Mertol Tüfekci, Yekai Sun, Jie Yuan, Chris Maharaj, Haibao Liu, John P. Dear, Loïc Salles

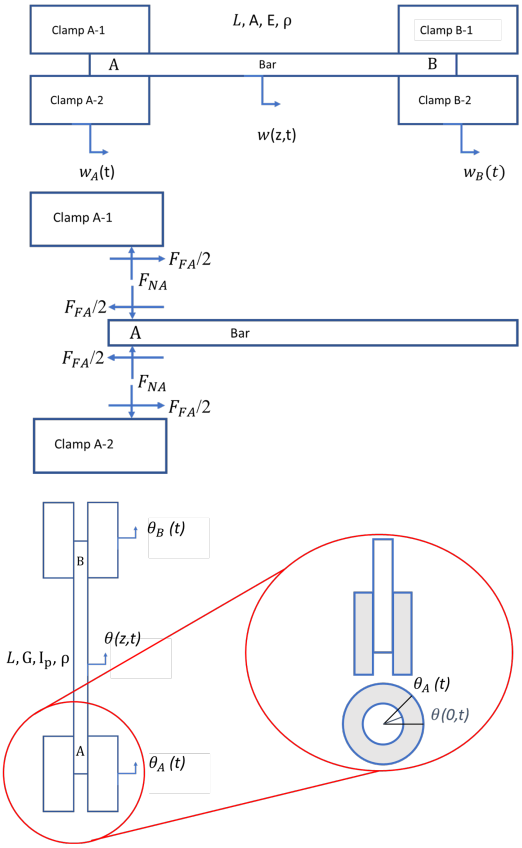

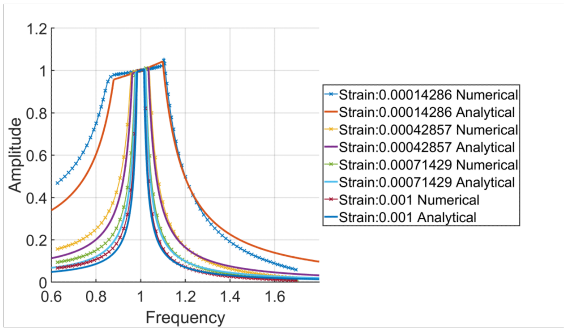

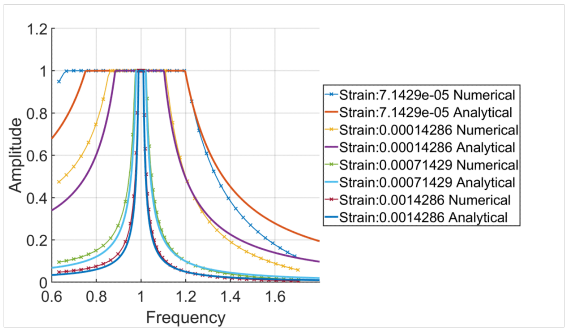

Analytical Vibration Modelling and Solution of Bars with Frictional Clamps

Mertol Tüfekci[a,*], Yekai Sun[a], Jie Yuan[b], Chris Maharaj[c], Haibao Liu[d], John P. Dear[a,*], Loïc Salles[e]

[a]*Department of Mechanical Engineering, Imperial College London, South Kensington Campus, London, SW7 2AZ, UK*
[b]*Computation Engineering Design Group, Department of Aeronautics and Astronautics, University of Southampton, S017 1BJ, UK*
[c]*Department of Mechanical and Manufacturing Engineering, The University of the West Indies, St. Augustine, REPUBLIC OF TRINIDAD AND TOBAGO*
[d]*School of Engineering and Materials Science, Queen Mary University of London, Mile End Road, London, E1 4NS, UK*
[e]*Department of Aerospace and Mechanical Engineering, University of Liège, Liège, 4000, BELGIUM*

Abstract

The present study introduces a novel analytical solution to predict the nonlinear dynamic behaviour of bars under frictional clamping in axial and torsional motions. It investigates the vibration characteristics of straight bars with imperfect supports, which introduce dry friction at their contact interfaces. The bars are tightly clamped between rigid fixtures, with the tightening load acting as a normal load that induces friction, thus adding nonlinearity to the system. The model simplifies contact forces to point loads and utilises both the Jenkins and velocity-dependent friction models for simulating contact friction. These frictional forces are represented as solution-dependent external forces in the governing differential equation for bar vibration, which also includes appropriate boundary conditions. The equation is solved both analytically and through the numerical method of alternating frequency-time harmonic balance, to explore the influence of contact parameters on the bar's support system behaviour. Comparisons between the numerical and analytical results demonstrate strong agreement, confirming the model's accuracy and validity.

Keywords: Bar vibrations, friction damping, nonlinear force, analytical solution, frequency response

1. Introduction

Damping is a crucial factor in governing the vibration response of a mechanical system. Friction joints are present in almost any engineering system: assembly joints of the different components in aircraft wings, friction in robotic arms' joints, contact between blades and disks in an aircraft engine and friction between the wires of bridge cables. Bridge cables are an example of friction between rods. Beam/bars are very popular elements used in mechanical systems. Their simple shape makes them easy to manufacture and the computation of internal stress can be done using analytical methods which accelerates the computations and the design process significantly [1, 2, 3].

Beams and bars are the most common continuous mechanical structures that are representative of real-world applications. This simplicity makes their mechanical behaviour relatively easier to predict. The beams/bars display predictable mechanical behaviour due to the concise mathematical formulations that make them easier to develop. Also, the simplicity of the mathematical formulations makes it easier to develop analytical solutions [4, 5, 6]. This predictability makes these objects one of the most commonly used for experiments. Beams/bars have been widely used in many experimental studies to test hypotheses, and properties of new materials such as damping [7]. However, for most of the experimental setups, the beams are subjected to contact either through clamping or jointed connections that change the stiffness,

*Correspondence: M. Tüfekci, m.tufekci17@imperial.ac.uk, J. P. Dear, j.dear@imperial.ac.uk

damping levels and vibration behaviours of the experimental system due to the inherent friction interfaces [8].

Friction in jointed structures is one of the areas that has been actively researched for many years [9, 10]. A good example would be the Parthenon. The existence of contact between wooden pinned joints and the marble drums of the columns of the Parthenon introduces frictional damping to the structure, which helps to significantly reduce the stresses occurring during earthquakes [11, 12, 13]. Friction contributes to the damping mechanism by serving as a dissipative force that opposes relative motion between two surfaces in contact. This is particularly evident in jointed structures, where frictional forces work to dissipate the kinetic energy of oscillations into thermal energy, thereby damping the system [14, 15, 16]. At the microscopic level, irregularities on the surfaces in contact engage and disengage dynamically as the structure undergoes vibration. This interaction leads to hysteresis losses, where the path of energy input into the system does not coincide with the path of energy output, resulting in energy being irreversibly lost as heat [17].

The frictional forces are not constant but rather change according to the speed, load, and even the temperature of the joint, making the damping nonlinear in nature. Stick-slip behaviour is a common manifestation of such nonlinear frictional damping. During the 'stick' phase, the static friction force holds the two contacting surfaces together, storing potential energy in the system. As the system reaches a critical stress state, slippage occurs, rapidly converting the stored potential energy into kinetic and eventually thermal energy [17, 18, 19].

This frictional damping is significant not only in ancient structures like the Parthenon but also in modern engineering applications such as clamped beams or bars, where understanding these damping mechanisms is crucial for accurate characterisation and optimisation [14, 15, 20, 21].As one of the most common damping sources in clamped beam/bar setups, friction must be considered during the characterisation of damping and dynamical properties of new materials and structures [20, 21].

The contribution of friction to damping has been investigated analytically, numerically and experimentally [22, 23, 24, 25]. There are various techniques to model contact friction itself [15, 26]. Among these techniques, the expression of friction forces depending on slip velocity and/or displacement using functions such as Benson, Coulomb, and smooth Coulomb functions stand out in the literature [27, 28, 29, 30, 31].

Alternatively, friction introduces nonlinear vibration behaviour such as amplitude dependent vibration leading to more complicated solution procedure [32, 33]. Thus, the nonlinear systems are commonly linearised to reduce the complexities. However, this reduces the accuracy of the solution to some extent [29, 30, 34].

Imperfections like compliance of supports and friction at the contact interfaces of supports are therefore usually neglected [35, 36, 37]. However, these imperfections may cause significantly different mechanical behaviour than the idealised model [38]. Some of these imperfections are quite hard to predict because of the lack of insight into their actual governing mechanisms. Stochastic modelling is one of the standard techniques to address the uncertainties of these imperfections [39, 40, 41]. There are works exploring the effects of uncertainties that focus on supports for beam/bar structures, which model complex boundary conditions [42, 43]. A number of studies showed that friction as one of these imperfections plays a crucial role in influencing the mechanical behaviour of a beam/bar-clamp-support system significantly [44, 36, 45, 37, 46]. It must be predicted and modelled accurately to be able to design the systems that match the desired criteria. In most of the experimental test setups, friction can influence the results significantly by changing the stiffness and introducing damping. Prediction of the effects of friction is the main concern of this study. Contact is unavaoidable especially in material damping measurement test rigs where friction can contribute to the damping data. This phenomenon can be often seen in dynamic mechanical analysis (DMA) test setups [47, 48].

To avoid/minimise the effects of friction in experimental setups such as clamped bars or beams, one must predict it with reasonable accuracy. For this purpose, Shaw [20] explored the influence of dry friction on a dynamic system using a velocity-dependent, piece-wise function for friction force. Ionescu and Paumier [28] employed a slip displacement-dependent approach for elastic systems for static analyses.

Ahn and Barber [21] studied the effect of response contacts on cyclic loading. Riddoch et al. [49] dealt with discrete systems that are subjected to frictional damping and base excitation. Marino et al. explored the motion of a single degree of freedom system influenced by friction arising from cyclic wall motion through analytical means [50]. In a subsequent study, Marino and Cicirello also conducted experimental investigations on a comparable system [51]. Later, they extend their work to develop an analytical framework for delineating the boundaries of motion regimes in systems with multiple degrees of freedom [52]. Apart from discrete systems, there are studies that examined continuous systems like bars/beams subjected to friction. Asadi et al. [45] investigated a beam supported with a bolted structure where friction is observed, both analytically and experimentally. Ferri and Bindermann [36] solve multiple cases where there is friction introduced by different types of supports. Apart from the frictional supports, there are also studies focusing on the dynamics of the beams touching a wall that causes friction [53, 46]. However, there are no analytical solutions to solve the axial and torsional dynamics of clamping bars including friction interfaces due to the complex non-smooth nonlinearities.

This study builds on the previous DMA research [54, 55] where the testing can be significantly affected by clamping bars with friction interfaces. This paper aims to develop an analytical formulation and solution to represent the axial and torsional vibration behaviour of bars with frictional supports in an efficient way. It is the first time such a nonlinear analytical solution is derived for the clamping bars with friction interfaces. The proposed analytical solution will efficiently quantify the effects of the friction on the clamping bars without the need for using the finite element (FE) modeling approach.

In this study, a novel approach is presented for understanding the vibration characteristics of straight bars with imperfect supports, particularly focusing on dry friction at contact interfaces during axial and torsional motions. Employing both Jenkins and velocity-dependent models, the frictional forces are meticulously modelled and integrated into the governing differential equation of the bar's vibrations as solution-dependent external loads. Uniquely, the study utilises the Galerkin method for analytical solution derivation, which allows the modelling of bars that have friction at clamps attached to them, alongside the traditional numerical method of alternating frequency-time harmonic balance (AFTHB) [56, 57, 58, 59, 60]. The findings display good consistency between the numerical and analytical models, substantiating the efficacy of the proposed approach. Notably, this research pioneers an efficient predictive framework for comprehensively characterising the dynamic behaviour of frictional bar-clamp systems undergoing both axial and torsional motions.

This paper is organised to offer an in-depth analysis of frictional damping in jointed structures. It pays special attention to the physical structure and the mathematical formulation, aiming for precise analytical and computational modelling. The following section delineates the governing equations and assumptions. Section 3, 'Analytical Solution' unveils a new framework for addressing the problem using analytical methods that leads to derivation of exact solutions. This is validated in the 'Numerical Modelling' section, which employs computational techniques to affirm the analytical findings.

2. Formulation of the Problem

This section presents the mathematical framework that governs the vibration characteristics of straight bars with imperfect supports influenced by dry friction. It begins with the 'Description of Problem and Assumptions', where the general problem is outlined along with the assumptions made for simplification. Subsequently, two distinct yet related mathematical models are introduced: one for 'Axial Motion' and another for 'Torsional Motion'. Each model is carefully formulated to account for the complexities introduced by frictional forces at the contact interfaces. The detailed mathematical expressions serve as the foundation for the analytical and numerical solutions discussed in subsequent sections.

2.1. Description of the Problem and Assumptions

The bar, with length L, cross-sectional area A material density ρ, is assumed to be made of linearly elastic, with elastic modulus E, homogeneous and isotropic material without any inherent material damping. Moreover, it is assumed that the vibration amplitude is small, the slip at the contact interfaces is

small as well. There is no micro slip, and no contact separation occurs throughout the entire motion. The friction force is mainly defined by the dependency of relative slip and slip velocity. The coefficient of friction is assumed to be constant and independent of the slip distance and the slip velocity. The normal loads at the contact interfaces is also simplified as concentrated point loads in this model.

2.2. Model in Axial Motion

The first formulation concerns the axial vibrations of a bar as one of the simplest cases for bars. This system is representative of the tension-compression fixture configuration of a DMA experiment setup. The axial models consist of a clamped-clamped bar, including friction at the interfaces between the bar surfaces and the clamps on both ends of the bar. A free body diagram is displayed in Figure 1 to show the interaction forces, and some dimensions where μ is the coefficient of friction between the clamps and the bar, F_{NA} and F_{NB} are the clamp tightening forces, evaluated as normal forces for friction modelling. The subscripts A and B notate the points where the friction exists. The forces are defined as functions of the friction coefficient, slip and slip velocity and the normal force, which is the tightening force for this model. Based on this free body diagram, an analytical model is formulated. Apart from the general assumptions enumerated earlier, this model is derived for distinct full-stick/full-slip (gross slip) motion regimes and assumes that the clamps are rigid and introduce tightening forces and friction as point loads.

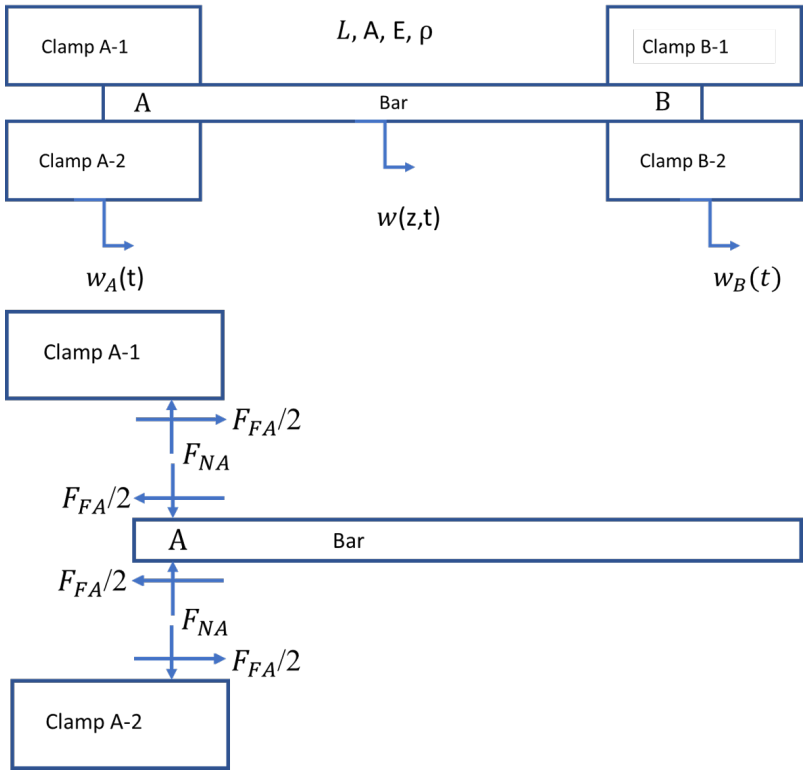

Figure 1: Axial forced vibration of a rod with frictional clamps.

The governing partial differential equation is the starting point for this analytical model. Relying on the assumptions described before, the wave equation is used as given:

$$\rho A\left(z\right)\frac{\partial^2 w}{\partial t^2}=\frac{\partial}{\partial z}\left[EA\left(z\right)\frac{\partial w}{\partial z}\right]+f\left(z,t\right) \tag{1}$$

where L is the length of the bar which lies between the clamps, A is the cross-sectional area of the bar, E is the modulus of elasticity, ρ is the density of the bar material, $f(z,t)$ is the external distributed load and $w(z,t)$ is the axial displacement of the bar.

The nonlinear part of this equation is the force term. As shown in the equation below, the frictional forces are expressed within the external load term.

$$f(z,t) = \delta(z)\, F_{FA} + \delta(z-L)\, F_{FB} \tag{2}$$

Here, $\delta(z)$ is the Dirac delta function. Also, F_{FA} and F_{FB} denote the friction forces applied by the clamps A and B on the bar.

The friction depends on the relative slip or slip velocity dependency, which are denoted with W_{slip} and $\dot{W}_{slip}$ respectively. The relative slip and slip velocities are expressed with respect to their locations, namely, points A and B as follows:

$$W_{A\ slip} = w(0,t) - w_A(t), \quad W_{B\ slip} = w(L,t) - w_B(t) \tag{3}$$

$$\dot{W}_{A\ slip} = \dot{w}(0,t) - \dot{W}_A(t), \quad \dot{W}_{B\ slip} = \dot{w}(L,t) - \dot{W}_B(t) \tag{4}$$

where $\dot{w}$ expresses the axial velocity of the bar, W_A, W_B, $\dot{W}_A$ and $\dot{W}_B$ express the displacement and velocity of the clamps respectively.

The interactions due to contact appear in the form of distributed loads. Their resultants are the effective frictional loads that are modelled as point loads/concentrated forces and/or moments. Acknowledging that this model aims to reduce the contact interactions into concentrated loads, the distributed loads need to be related to concentrated loads in terms of the contact parameters. The contact pressure p is the reason for the resulting normal force at the contact, and τ is the frictional shear stress which leads to the tangential frictional force when summed over the contact surface area A^*. The relations between the contact forces, pressure and shear are expressed as:

$$F_{FA} = \int_A \tau_A \, dz \ , \quad F_{FB} = \int_A \tau_B \, dz \tag{5}$$

$$F_{NA} = \int_A p_A \, dz \ , \quad F_{NB} = \int_A p_B \, dz \tag{6}$$

The contact pressure and shear are related as a function of the friction coefficient, contact pressure and relative slip or slip velocity, depending on the friction model used.

Finally, the governing equation of motion is transformed into the following form, which is a wave equation with a nonlinear external force term.

$$\rho A(z) \frac{\partial^2 w}{\partial t^2} = \frac{\partial}{\partial z}\left[EA(z)\frac{\partial w}{\partial z}\right] + \delta(z)\ F_{FA} + \delta(z-L)\ F_{FB} \tag{7}$$

2.3. Model in Torsional Motion

In this scenario, the friction involved in the torsional vibration of a bar is formulated. For the sake of simplicity, the model is formulated for a bar with a straight axis and a circular cross-section. More specifically, this model is derived for cylindrical bars and not for arbitrarily prismatic ones. The formulation of torsional vibrations of bars is based on the same assumptions and the same form of governing equation below, as the axial case. Figure 2 presents a simple cylindrical bar, fitted into pipes, which behave as clamps, with initial fitting pressures p_A and p_B along the lengths of the contacting regions of the clamps l_A and l_B, which are not considered in the free bar length L.

$$\rho I_p(z) \frac{\partial^2 \theta}{\partial t^2} = \frac{\partial}{\partial z}\left[GI_t(z)\frac{\partial \theta}{\partial z}\right] + m(z,t) \tag{8}$$

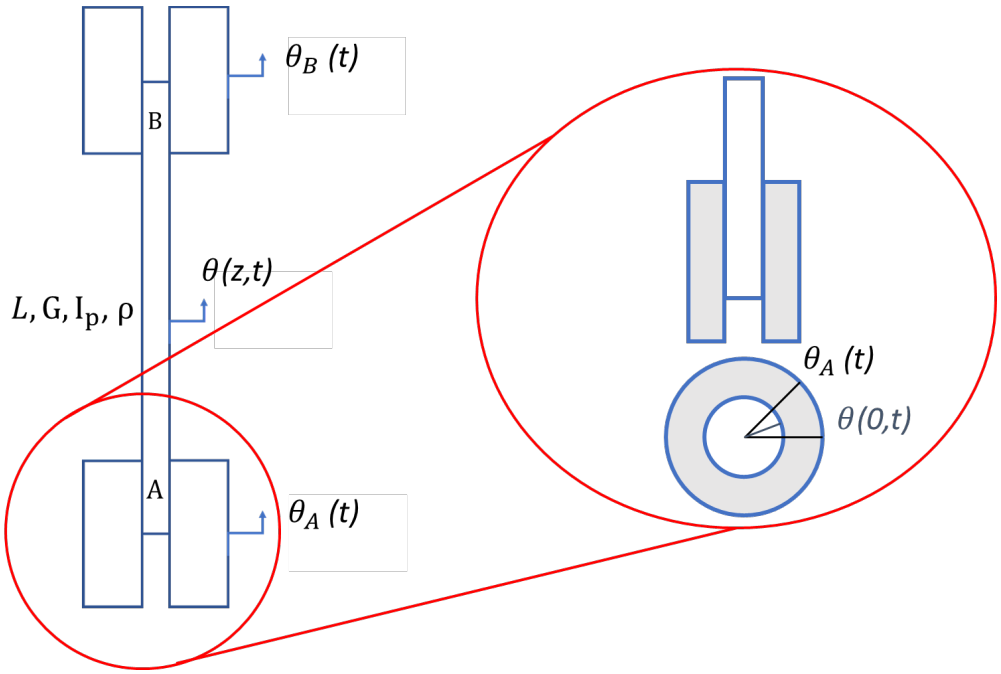

Figure 2: Circular bar fitted in a pipe for clamping.

where, I_t is the torsional moment of inertia, I_p is the polar area moment of inertia, G is the shear modulus of the material, $m(z,t)$ is the external distributed torsional moment term, and θ is the twist angle the bar. Considering that the bar has a circular cross-section, I_t becomes I_p.

Assuming the external loads as point loads, the load term becomes:

$$m(z,t) = \delta(z) M_{FA} + \delta(z-L) M_{FB} \tag{9}$$

Here, M_{FA} and M_{FB} are the resultant moments applied on the bar by the fittings.

For further analysis, the loads acting on the bar are displayed in Figure 3. As mentioned earlier, p is the fitting pressure, while τ is the shear caused by the friction at the contact interface.

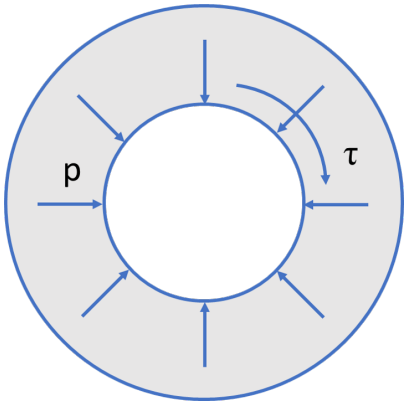

Figure 3: Contact pressure and tangential distributed load at the contact interface for fitted circular bar

Using the relevant friction models, the relation between the shear and the contact pressure is the same as in the axial case given in Equations (5) and (6).

To calculate the resulting moment, the contact friction shear is to be integrated over the whole surface of contact. This integration is shown as:

$$M_{FA} = \int_0^{l_A} \tau_A \ \pi \ D \ dz \ , \quad M_{FB} = \int_0^{l_B} \tau_B \ \pi \ D \ dz \tag{10}$$

Using the moment terms in the governing equation of motion, the expression becomes:

$$\begin{aligned} \rho I_p(z) \frac{\partial^2 \theta}{\partial t^2} = \frac{\partial}{\partial z}\left[G I_p(z) \frac{\partial \theta}{\partial z} \right] + \delta(z) \int_0^{l_A} \tau_A \ \pi \ D \ dz \\ + \delta(z-L) \int_0^{l_B} \tau_B \ \pi \ D \ dz \end{aligned} \tag{11}$$

3. Analytical Solution

In this section, a new analytical solution is proposed to solve the axial and torsional formulations with friction forces presented in Section 2. The displacement (Jenkins) and the velocity-dependent friction models are used to represent the behaviour of frictional contact forces on the clamping interfaces. It is assumed that the first vibration mode of the bar is dominant to the response of the bar. Besides, it is considered that the clamps are identical, and have the same tightening force. Also, the clamps move with the same frequency and amplitude but in reverse directions, which cause the midpoint of the bar to be stationary despite the nonlinearity introduced by the frictional contact. Hence, the system shows a symmetry around the middle of the bar. This allows for simplification of the model by evaluating only half of the bar. This simplified model is then nondimensionalised to generalise the solution procedure and the results.

3.1. Axial Model

The clamped bar model with moving clamps in the axial direction introduced in the previous section (Section 2.2) is studied in detail here. Referring to Figure 4a and Figure 4b, the frictional clamp (initially at $z = L$) is assumed to move with a harmonic displacement $a\cos(\Omega t)$ and to exert a contact force at the tip of the clamped free bar. This is half of the model described in the formulation section. Taking advantage of the symmetry assumption explained earlier, only half of the bar is representative of the actual system.

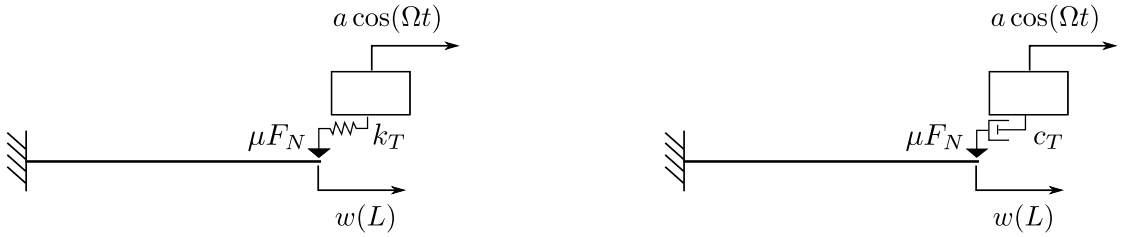

(a) Axial problem with Jenkins element at the tip of the clamped free bar.

(b) Axial problem with velocity-dependent element at the tip of the clamped free bar.

Figure 4: Axial problem with clamped and fixed and bar.

3.1.1. Nondimensionalisation

If one assumes that a constant cross-sectional and material properties throughout the bar and the imposed displacement to the clamp be equal to $a\cos(\Omega t)$, the equation of motion for the axial model, where $w(\bar{z}, t)$ is the axial displacement of the bar, is transformed into the form presented below, which is a simplified version of Equation (7).

$$\rho A \frac{\partial^2 w}{\partial t^2} - EA \frac{\partial^2 w}{\partial z^2} = \delta(z-L) \ F_{NL}(w_{rel}, \frac{\partial w_{rel}}{\partial t}) \tag{12}$$

As explained earlier, taking advantage of the symmetry, the boundary condition for the stationary point in the middle of the bar can be expressed as:

$$w(0,t) = 0 \tag{13}$$

The previous equation is nondimensionalised using the following variables: $\tilde{w}$, $\tilde{t}$, $\tilde{\Omega}$, $\tilde{F}$, $\tilde{k}$, $\tilde{c}$, $\tilde{\kappa}$, $\tilde{\kappa}_0$, $\tilde{k}_T$, and $\tilde{c}_T$, obtained as:

$$\begin{aligned} m = \rho A L \ ; \ \kappa = \omega\sqrt{\rho/E} \ ; \ \kappa_0 = \omega_0\sqrt{\rho/E} \ ; \ F_0 = m\,\omega_0^2 a \\ k_0 = m\,\omega_0^2 \ ; \ c_0 = m\,\omega_0 \ ; \ \tilde{w} \ = \ w/a \ ; \ \tilde{z} \ = \ z/L \ ; \ \tilde{t} \ = \ t\,\omega_0 \\ \tilde{\Omega} \ = \ \Omega/\omega_0 \ ; \ \tilde{F} \ = \ F/F_0 \ ; \ \tilde{k} \ = \ k/k_0 \ ; \ \tilde{c} \ = \ c/c_0 \ ; \ \tilde{\kappa} \ = \ \kappa L \\ \tilde{\kappa}_0 = \kappa_0 L \ ; \ \tilde{k}_T \ = \ k_T/k_0 \ ; \ \tilde{c}_T \ = \ c_T/c_0 \end{aligned} \tag{14}$$

where a is the amplitude of the clamp motion, m is the mass, A is the cross-sectional area and L is the length of the bar, ω_0 is the eigenvalue of the bar mode one wants to study, $1/\kappa$ is the wavelength of the excited frequency, $1/\kappa_0$ is the wavelength of the corresponding eigenfunction, F_0 is the characteristic force, k_0 is the characteristic stiffness, c_0 is the characteristic damping, k_T is the stiffness coefficient of the contact and c_T is the damping coefficient of the contact.

Finally, multiplying Equation (12) by the factor $1/(\rho A\omega_0^2 a)$ and making the scaled variables appear reads as follows:

$$\ddot{\tilde{w}} - \frac{1}{\tilde{\kappa}_0^2}\tilde{w}'' = \delta(\tilde{z}-1)\ \tilde{F}_{NL} \tag{15}$$

where $\tilde{F}_{NL}$ indicates the nonlinear force which corresponds to frictional force, $\ddot{\tilde{w}} = \frac{\partial^2 \tilde{w}}{\partial \tilde{t}^2}$, $\tilde{w}'' = \frac{\partial^2 \tilde{w}}{\partial \tilde{z}^2}$, and the transformation of the Dirac delta from $\delta(z-L)$ to $\delta(\tilde{z}-1)$ generated a factor L.

To solve this problem, it is assumed that the harmonic displacement of the clamp has a frequency around the first natural frequency of the bar. Hence, the ansatz is shown:

$$\tilde{w}(\tilde{z},\tilde{t}) = \alpha \sin(\tilde{\kappa}\tilde{z})\cos(\tilde{\Omega}\tilde{t}+\psi) \tag{16}$$

$\tilde{w}$ is the nondimensional displacement, α is the nondimensional amplitude of the bar motion over the nondimensional amplitude of the clamp motion, and ψ is the phase.

The application Galerkin method i.e. the projection of Equation (15) onto the shape function $\sin(\tilde{\kappa_0}^2)$, leads to:

$$\frac{1}{2}\,\alpha^2(1-\tilde{\Omega}^2)\cos(\tilde{\Omega}\tilde{t}+\psi) = \tilde{F}_{NL} \tag{17}$$

The nondimensional relative displacement of the bar by the clamp (at $\tilde{z}=1$) is presented below:

$$\tilde{w}_{rel}(\tilde{t}) = \cos(\tilde{\Omega}\tilde{t}) - \alpha\cos(\tilde{\Omega}\tilde{t}+\psi) \tag{18}$$

Also, the amplitude of this relative displacement is expressed:

$$\alpha_{rel} = \sqrt{1+\alpha^2-2\,\alpha\cos(\psi)} \tag{19}$$

3.1.2. Jenkins Element

When using the Jenkins approach, there is a limit to the relative slip displacement up to which the frictional dissipation at the bar-clamp interface can be avoided. If the clamp is modelled with a Jenkins element, the stick limit condition for the amplitude yields:

$$\tilde{k}_T \; \alpha^*_{rel} = \mu \tilde{F}_N \tag{20}$$

where α^*_{rel} is the relative amplitude at the stick limit, and if the actual amplitude of the bar does not exceed the limit, $\alpha_{rel} \leq \alpha^*_{rel}$ the contact force becomes linear because the clamp is in full-stick. Thus, F_{NL} becomes as presented:

$$\tilde{F}_{NL}(\tilde{t}) = \tilde{k}_T \, \tilde{w}_{rel}(\tilde{t}) \tag{21}$$

Under these conditions, one can solve Equation (17) in the unknown α and ψ by projection onto $\sin(\tilde{\Omega}\tilde{t} + \psi)$ and $\cos(\tilde{\Omega}\tilde{t} + \psi)$, that reads as shown:

$$\alpha = \frac{2\tilde{k}_T}{1 - \tilde{\Omega}^2 + 2\tilde{k}_T} \tag{22a}$$

$$\psi = 0 \tag{22b}$$

$$\alpha_{rel} = |1 - \alpha| = \left| \frac{1 - \tilde{\Omega}^2}{1 - \tilde{\Omega}^2 + 2\tilde{k}_T} \right| \tag{22c}$$

Imposing the condition $\alpha_{rel} \leq \alpha^*_{rel}$, which leads to the expression for α^*_{rel} :

$$\alpha^*_{rel} = \frac{\mu \tilde{F}_N}{\tilde{k}_T} \tag{23}$$

One can derive an expression for the range of $\tilde{\Omega} \in [\tilde{\Omega}_{*pre}, \tilde{\Omega}_{*post}]$ where the full-stick regime occurs and the values of the full-stick region limits. This yields the following equation:

$$\tilde{\Omega}_{*pre} = \sqrt{1 - 2\,\tilde{k}_T \, \frac{\mu \tilde{F}_N}{\tilde{k}_T - \mu \tilde{F}_N}} \tag{24a}$$

$$\tilde{\Omega}_{*post} = \sqrt{1 + 2\,\tilde{k}_T \, \frac{\mu \tilde{F}_N}{\tilde{k}_T + \mu \tilde{F}_N}}. \tag{24b}$$

Similarly, the corresponding vibration amplitudes are obtained as given:

$$\alpha_{*pre} = 1 - \frac{\mu \tilde{F}_N}{\tilde{k}_T} \tag{25a}$$

$$\alpha_{*post} = 1 + \frac{\mu \tilde{F}_N}{\tilde{k}_T} \tag{25b}$$

The slip condition is represented with a simplified approach. For the cases where there is slip, it is assumed that the system is excited with force, which has a maximum of $\mu \tilde{F}_N$. Considering the harmonic motion of the clamps, it can be stated that the excitation force is harmonic, and its amplitude is $\mu \tilde{F}_N$ as described in Section 4.1.1. Thus, the system becomes linear with a solution for this particular region

3.1.3. Velocity-Dependent Element

Dissipation in the clamp is always present with the velocity-dependent model, but frictional dissipation only occurs if the relative slip velocity exceeds the stick limit. In this case, the stick limit condition reads as shown below:

$$\tilde{c}_T\,\tilde{\Omega}\alpha^*_{rel} = \mu\tilde{F}_N \tag{26}$$

where c_t is the damping coefficient of the frictional contact.

Because the clamp is in full-stick as Jenkins model if $\alpha_{rel} \leq \alpha^*_{rel}$, the contact force becomes linear. This is expressed as:

$$\tilde{F}_{NL}(\tilde{t}) = \tilde{c}_T\,\dot{\tilde{w}}_{rel}(\tilde{t}) \tag{27}$$

Solving Equation (17) in the unknown α and ψ by projection onto $\sin(\tilde{\Omega}\tilde{t}+\psi)$ and $\cos(\tilde{\Omega}\tilde{t}+\psi)$, that yields the results which are shown:

$$\alpha = \frac{2\,\tilde{c}_T\,\tilde{\Omega}}{\sqrt{(1-\tilde{\Omega}^2)^2 + (2\,\tilde{c}_T\,\tilde{\Omega})^2}}, \tag{28a}$$

$$\psi = \arctan\left(\frac{1-\tilde{\Omega}^2}{2\,\tilde{c}_T\,\tilde{\Omega}}\right), \tag{28b}$$

$$\alpha_{rel} = \frac{|1-\tilde{\Omega}^2|}{\sqrt{(1-\tilde{\Omega}^2)^2 + (2\,\tilde{c}_T\,\tilde{\Omega})^2}} \tag{28c}$$

Imposing the condition $\alpha_{rel} \leq \alpha^*_{rel}$, one could derive an expression for the range of $\tilde{\Omega} \in [\tilde{\Omega}_{*pre}, \tilde{\Omega}_{*post}]$ where the full-stick regime occurs and the values of the full-stick region limits. To obtain a simplified expression, an approximation on the equation for α_{rel} can be done, assuming that the term $\tilde{c}_T\tilde{\Omega} \approx \tilde{c}_T\bar{\Omega}$ does not vary with $\tilde{\Omega}$. The expressions under this assumption are displayed as follows:

$$\tilde{\Omega}_{*pre} = \sqrt{1 - \frac{2\tilde{c}_T\,\bar{\Omega}\mu\tilde{F}_N}{\sqrt{(\tilde{c}_T\bar{\Omega})^2 - (\mu\tilde{F}_N)^2}}}. \tag{29a}$$

$$\tilde{\Omega}_{*post} = \sqrt{1 + \frac{2\tilde{c}_T\,\bar{\Omega}\mu\tilde{F}_N}{\sqrt{(\tilde{c}_T\bar{\Omega})^2 - (\mu\tilde{F}_N)^2}}}. \tag{29b}$$

Similarly the corresponding vibration amplitudes are formulated:

$$\alpha_{*pre} = \alpha_{*post} = \sqrt{1 - \left(\frac{\mu\tilde{F}_N}{\tilde{c}_T\bar{\Omega}}\right)^2} \tag{30}$$

Similar to the case with the Jenkins model, for the regimes other than full-stick, in other words, where slip occurs, the same assumption is made for harmonic force excitation.

3.2. Torsional Model

The bar model in torsional motion, described in the previous section (Section 2.3), is solved following the same steps for the axial case (Section 3.2). Considering that the form of the governing equation is the same as the axial model, the solution procedures are pretty similar. Besides, like the axial model,

here, the clamps at both ends of the bar are assumed to move with the same frequency but in opposite directions, obeying the harmonic displacement function $\theta_A \cos(\Omega t)$ and $\theta_B \cos(\Omega t - \pi)$. Here, θ_A is the rotation amplitude and Ω is the frequency of the clamp motion. This enables one to model half of the bar to simplify the model, taking advantage of the stationary middle point of the bar. The motion of these clamps applies frictional forces on the bar that results in net moments, which force the bar in torsion. As with the axial model, both Jenkins and velocity-dependent friction models are applied, and the analytical solutions are obtained.

3.2.1. Nondimensionalisation

Assuming a constant circular cross-section and the imposed displacement onto the clamps that are initially at $z = L$ to be equal to $\theta_A \cos(\Omega t)$, the equation of the torsional rotation $\theta(\bar{z}, t)$ is formed into using Equation (11).

$$\rho I_p \frac{\partial^2 \theta}{\partial t^2} - G I_p \frac{\partial^2 \theta}{\partial z^2} = \delta(z - L)\ M_{NL} \tag{31}$$

For normalisation, the nondimensional variables $\tilde{r}$, $\tilde{\theta}$, $\tilde{t}$, $\tilde{\Omega}$, $\tilde{M}$, $\tilde{k}$, $\tilde{c}$, $\tilde{\kappa}$, $\tilde{\kappa}_0$ $\tilde{k}_T$ and $\tilde{c}_T$ are defined as:

$$\begin{gathered} r_0 = r\theta_A\ ,\ J = \rho I_p\ ;\ \kappa = \omega\sqrt{\rho/G}\ ;\ \kappa_0 = \omega_0\sqrt{\rho/G} \\ M_0 = J\,\omega_0^2\ L\ \theta_A\ ;\ k_0 = J\,\omega_0^2\ L\ ;\ c_0 = J\,\omega_0\ L\ ;\ \tilde{r} = r/r_0\ ;\ \tilde{\theta}\ =\ \theta/\theta_A \\ \tilde{z}\ =\ z/L\ ;\ \tilde{t}\ =\ t\,\omega_0\ ;\ \tilde{\Omega}\ =\ \Omega/\omega_0\ ;\ \tilde{M}\ =\ M/M_0\ ;\ \tilde{k}\ =\ k/k_0 \\ \tilde{c}\ =\ c/c_0\ ;\ \tilde{\kappa}\ =\ \kappa L;\ \tilde{\kappa}_0 = \kappa_0 L\ ;\ \tilde{k}_T\ =\ k_T/k_0\ ;\ \tilde{c}_T\ =\ c_T/c_0 \end{gathered} \tag{32}$$

where the system parameters are the mass moment of inertia J, the cross-sectional polar area moment of inertia I_p and the rest of the parameters are defined as explained in the previous section where the axial case is solved.

Multiplying Equation (31) by the factor $1/(J\omega_0^2\theta_A)$ and displaying the normalised variables, the following expression is obtained:

$$\ddot{\tilde{\theta}} - \frac{1}{\tilde{\kappa}_0^2}\tilde{\theta}'' = \delta(\tilde{z} - 1)\ \tilde{M}_{NL} \tag{33}$$

where $\ddot{\tilde{\theta}} = \frac{\partial^2 \tilde{\theta}}{\partial \tilde{t}^2}$, $\tilde{\theta}'' = \frac{\partial^2 \tilde{\theta}}{\partial \tilde{z}^2}$, and the Dirac delta transforms from $\delta(z - L)$ to $\delta(\tilde{z} - 1)$ by generating a factor L.

The clamps move following a harmonic rotation function with a range of frequency around the first torsional natural frequency of the bar. In the ansatz shown in the equation below, the function $\tilde{\theta}$ stands for the nondimensional rotation and α for the nondimensional amplitude of the bar motion over the amplitude of the clamp motion.

$$\tilde{\theta}(\tilde{z}, \tilde{t}) = \alpha \sin(\kappa\tilde{z}) \cos(\tilde{\Omega}\tilde{t} + \psi) \tag{34}$$

Applying the Galerkin method i.e. the projection of Equation (33) onto the shape function $\sin(\frac{\pi\tilde{z}}{2})$, leads to Equation (35)

$$\frac{1}{2}\,\alpha^2(1 - \tilde{\Omega}^2)\cos(\tilde{\Omega}\tilde{t} + \psi) = \tilde{M}_{NL} \tag{35}$$

The nondimensional relative rotation at $\tilde{z} = 1$ and its amplitude are given in the equations below:

$$\tilde{\theta}_{rel}(\tilde{t}) = \cos(\tilde{\Omega}t) - \alpha\cos(\tilde{\Omega}\tilde{t} + \psi) \tag{36}$$

$$\alpha_{rel} = \sqrt{1 + \alpha^2 - 2\,\alpha\cos(\psi)} \tag{37}$$

3.2.2. Jenkins Element

Similar to the axial case, the stick limit condition is expressed as:

$$\tilde{k}_T \ \alpha^*_{rel} = \mu \tilde{F}_N \tilde{r} \tag{38}$$

where α^*_{rel} is the nondimensional relative rotation amplitude at the stick limit. In the case where the amplitude remains below the limit, $\alpha_{rel} \leq \alpha^*_{rel}$ the contact force and consecutively, the moment becomes linear because the clamp stays in the full-stick regime.

Hence, F_{NL} and M_{NL} become:

$$\tilde{F}_{NL}(\tilde{t}) = \frac{\tilde{k}_T \, \tilde{\theta}_{rel}(\tilde{t})}{\tilde{r}} \tag{39a}$$

$$\tilde{M}_{NL}(\tilde{t}) = \tilde{k}_T \, \tilde{\theta}_{rel}(\tilde{t}) \tag{39b}$$

It then becomes possible to solve Equation (35) in the unknown α and ψ using the same philosophy as the axial case. The resulting expressions are shown:

$$\alpha = \frac{2\tilde{k}_T}{1 - \tilde{\Omega}^2 + 2\tilde{k}_T} \tag{40a}$$

$$\psi = 0 \tag{40b}$$

$$\alpha_{rel} = |1 - \alpha| = \left| \frac{1 - \tilde{\Omega}^2}{1 - \tilde{\Omega}^2 + 2\tilde{k}_T} \right| \tag{40c}$$

dFor the condition $\alpha_{rel} \leq \alpha^*_{rel}$, the expressions for the range of the full-stick regime and the limit values of the full-stick region $\tilde{\Omega} \in [\tilde{\Omega}_{*pre}, \tilde{\Omega}_{*post}]$ are found as well as the amplitudes. These are given in the following equations:

$$\tilde{\Omega}_{*pre} = \sqrt{1 - 2\,\tilde{k}_T \, \frac{\mu \tilde{F}_N \tilde{r}}{\tilde{k}_T - \mu \tilde{F}_N \tilde{r}}} \tag{41a}$$

$$\tilde{\Omega}_{*post} = \sqrt{1 + 2\,\tilde{k}_T \, \frac{\mu \tilde{F}_N \tilde{r}}{\tilde{k}_T + \mu \tilde{F}_N \tilde{r}}}. \tag{41b}$$

$$\alpha_{*pre} = 1 - \frac{\mu \tilde{F}_N \tilde{r}}{\tilde{k}_T} \tag{42a}$$

$$\alpha_{*post} = 1 + \frac{\mu \tilde{F}_N \tilde{r}}{\tilde{k}_T} \tag{42b}$$

The final possible condition is when clamps fail to stick to the bar surface and slide. The same assumption is made as in Section 3.1.2. This suggests that the bar is excited in the torsional direction with a harmonic moment and an amplitude of $\mu \tilde{F}_N \tilde{r}$ since the clamps rotate following a harmonic function.

3.2.3. Velocity-Dependent Element

Developing the model with the velocity-dependent formulation leads to the stick limit condition shown as:

$$\tilde{c}_T\,\tilde{\Omega}\alpha^*_{rel} = \mu\tilde{F}_N\tilde{r} \tag{43}$$

where c_T is the damping coefficient of the frictional contact.

$\alpha_{rel} \leq \alpha^*_{rel}$ makes the contact force linear because the clamp sticks fully similar to the Jenkins model. This is given as:

$$\tilde{F}_{NL}(\tilde{t}) = \tilde{c}_T\,\dot{\tilde{\theta}}_{rel}(\tilde{t})\tilde{r} \tag{44a}$$

$$\tilde{M}_{NL}(\tilde{t}) = \tilde{c}_T\,\dot{\tilde{\theta}}_{rel}(\tilde{t}) \tag{44b}$$

To solve Equation (35) for the unknown α and ψ by projection onto $\sin(\tilde{\Omega}\tilde{t}+\psi)$ and $\cos(\tilde{\Omega}\tilde{t}+\psi)$, that lead to the results presented as follows:

$$\alpha = \frac{2\,\tilde{c}_T\,\tilde{\Omega}}{\sqrt{(1-\tilde{\Omega}^2)^2 + (2\,\tilde{c}_T\,\tilde{\Omega})^2}}, \tag{45a}$$

$$\psi = \arctan\left(\frac{1-\tilde{\Omega}^2}{2\,\tilde{c}_T\,\tilde{\Omega}}\right), \tag{45b}$$

$$\alpha_{rel} = \frac{|1-\tilde{\Omega}^2|}{\sqrt{(1-\tilde{\Omega}^2)^2 + (2\,\tilde{c}_T\,\tilde{\Omega})^2}} \tag{45c}$$

Considering the condition $\alpha_{rel} \leq \alpha^*_{rel}$, the expressions for the range of the full-stick regime and the values of the full-stick region limits $\tilde{\Omega} \in [\tilde{\Omega}_{*pre}, \tilde{\Omega}_{*post}]$ can be derived. For a simplified expression, one can assume that the term $\tilde{c}_T\tilde{\Omega} \approx \tilde{c}_T\bar{\Omega}$ does not vary with $\tilde{\Omega}$. The expressions under these assumptions read:

$$\tilde{\Omega}_{*pre} = \sqrt{1 - \frac{2\tilde{c}_T\,\bar{\Omega}\mu\tilde{F}_N\tilde{r}}{\sqrt{(\tilde{c}_T\bar{\Omega})^2 - (\mu\tilde{F}_N\tilde{r})^2}}}. \tag{46a}$$

$$\tilde{\Omega}_{*post} = \sqrt{1 + \frac{2\tilde{c}_T\,\bar{\Omega}\mu\tilde{F}_N\tilde{r}}{\sqrt{(\tilde{c}_T\bar{\Omega})^2 - (\mu\tilde{F}_N\tilde{r})^2}}}. \tag{46b}$$

The corresponding vibration amplitudes, shown below, are derived similarly.

$$\alpha_{*pre} = \alpha_{*post} = \sqrt{1 - \left(\frac{\mu\tilde{F}_N\tilde{r}}{\tilde{c}_T\bar{\Omega}}\right)^2} \tag{47}$$

To solve the sliding condition, the same approach is used with the previous models. Taking advantage of the harmonic motion of the clamps, a harmonic moment with the amplitude of $\mu\tilde{F}_N$ is chosen to stand for the excitation moment.

3.3. Selection of Solutions

As described previously, the analytical solutions are developed for the models considering full-stick and slip conditions. As a result, there are two separate solutions. The combinations of these two represent the solution for the nonlinear bar-clamp system. The question is, which regime solution is valid at the particular point of the domain. The valid expression for a particular excitation frequency is the one that requires less frictional contact force, in other words, the one that yields the lower amplitude.

Figure 5 shows some schematic curves for the required frictional force F_R, which reaches its minimum at the resonance frequency, and the maximum contact friction force F_{Fmax} against frequency assuming $F_{Fmax} = \mu F_N$. In Figure 5a, the first case is displayed, where these curves do not intersect, which means the necessary frictional contact force is always greater than the maximum contact friction force. This will always result in slip and consequently frictional dissipation along with the frequency interval of interest. The second case is visualised in Figure 5b where the required frictional contact forces are relatively lower so that there is only one intersection. In this case, the full-stick regime governs the system up until the intersection frequency and the slip regime takes over for the frequencies greater than that. Finally, as shown in Figure 5c, there can be two intersections of the presented curves. This leads to a domain divided into three regions, namely a full-stick regime between the intersection points and slip before the first and beyond the second point of intersection.

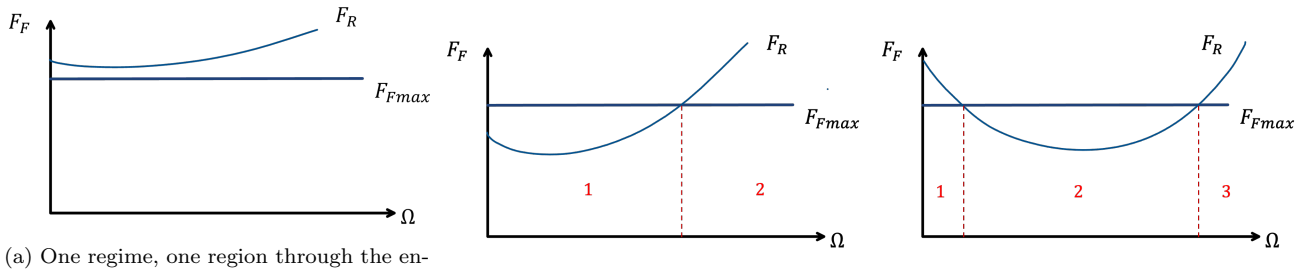

(a) One regime, one region through the entire frequency interval: Full-slip domination.

(b) Two regimes, two regions: Full-stick, full-slip.

(c) Two regimes, three regions: Full-slip, full-stick, full-slip.

Figure 5: Existence of regimes and regions based on the contact forces.

4. Numerical Modelling

The developed analytical solutions in the last section are compared to the numerical one using AFTHB [57, 61]. Both Jenkins and velocity-dependent friction models are used to simulate the nonlinear dynamic response of axial and torsional vibration bars. First, the definitions of the nonlinear friction forces are presented. Then, the numerical approach is briefly explained.

4.1. Nonlinear Friction Force Definition and Modelling

The friction models can be either defined in terms of the relative displacement between the two points in contact or the relative velocity. In both cases, the limit value that the nonlinear force assumes for large relative motion coincides with the tangential friction force μF_N. At very small values of the relative motion, the contact is instead modelled as a force in linear relation with the chosen variable (either relative displacement or relative velocity).

Such force is the contact force exerted by the clamp on the bar when the two components are considered to be in stuck conditions.

In both cases, $F_R(w_{rel}, \dot{w}_{rel})$ is defined as the frictional contact force, the expression of the nonlinear friction force is written as:

$$F_{NL}(w_{rel}, \dot{w}_{rel}) = \begin{cases} -\mu F_N & \text{if } F_R(w_{rel}, \dot{w}_{rel}) < -\mu F_N \\ +\mu F_N & \text{if } F_R(w_{rel}, \dot{w}_{rel}) > +\mu F_N \\ F_R(w_{rel}, \dot{w}_{rel}) & \text{else} \end{cases} \tag{48}$$

4.1.1. Jenkins Model

If the frictional contact force F_R is modelled with an elastic behaviour (displacement formulation, which is similar to a spring formulation), the resulting nonlinear element will coincide with a Jenkins element. Hence, the frictional contact force is given by:

$$F_R = k_T(w_{rel} - \Delta w_{slip}) \tag{49}$$

where k_T is the tangential contact stiffness and Δw_{slip} is the cumulative relative displacement accumulated during the slip phase. Numerically the value of Δw_{slip} is obtained through a time discretisation of the period, solving for the variables and updating the value of Δw_{slip} at each time step of the slip phase. An analytical expression cannot be provided for the general case, but it can be found if one assumes that the relative displacement is a purely harmonic function which is expressed as:

$$w_{rel}(t) = a\cos(\Omega t). \tag{50}$$

If the value of $k_T\, a$ exceeds the friction limit μF_N a stick-slip cycle is observed. Otherwise, the value of Δw_{slip} assumes the simple expression shown in the following equation:

$$\Delta w_{slip} = -\text{sign}(\dot{w}_{rel})(a - \frac{\mu F_N}{k_T}) \tag{51}$$

Being $\dot{w}_{rel} = -a\Omega\sin(\Omega t)$, for the first half period, the sign of the velocity will be negative, and for the second half, positive. The frictional contact force is written as:

$$F_R = \begin{cases} k_T\, a\cos(\Omega t) - (k_T\, a - \mu F_N) & \text{if } t \in [0, T/2] \\ k_T\, a\cos(\Omega t) + (k_T\, a - \mu F_N) & \text{if } t \in [T/2, T] \end{cases} . \tag{52}$$

where T indicates a vibration period.

Obviously, in the case of $k_T\, a < \mu F_N$, a full-stick cycle will occur. This means no dissipation is observed, and the frictional force is a purely elastic reaction.

The case of a generic stick-slip cycle is reported in Figure 6. One can notice that the four different conditions for the friction force are depicted with different colours, and the hysteresis loop generated is shown in the (b) plot. The area enclosed in the hysteresis loop, representing the dissipated energy, is equal to $2\mu F_N(a - \frac{\mu F_N}{k_T})$: for very small values of the friction limit, the cycle will mostly consist of slip phases and the energy dissipated will be small, and for $a \leq \frac{\mu F_N}{k_T}$ the cycle will reduce to a pure stick cycle with no dissipation.

Another notable observation is that for the generic case reported in Figure 6 the equivalent stiffness introduced in the system by the friction element is lower than k_T due to the presence of the slip phases. In the extreme case of a pure stick cycle, this stiffness will equal k_T, whereas in the extreme case of an almost full-slip cycle, it will tend to be zero.

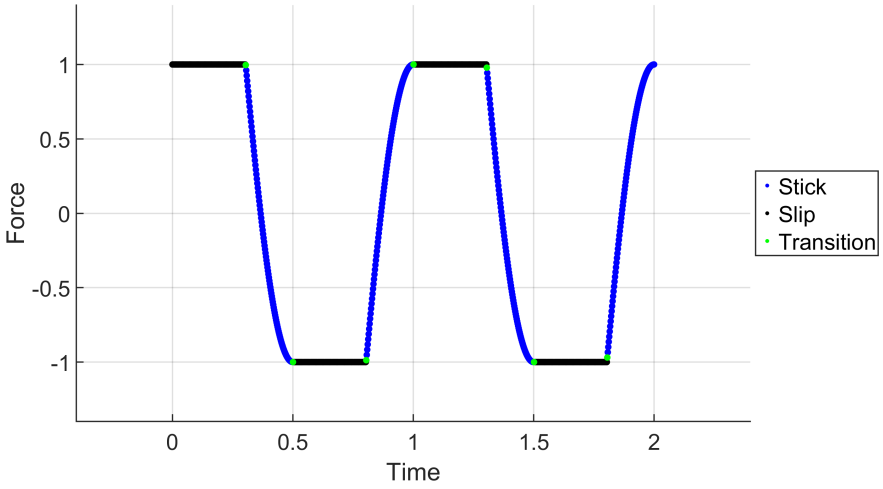

(a) Force against time.

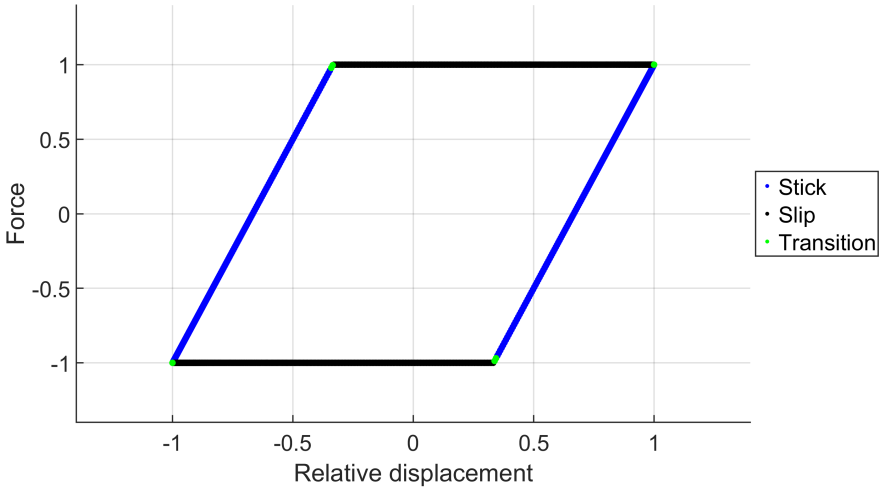

(b) Force against relative displacement.

Figure 6: Simplified Jenkins element under the single harmonic assumption.

4.1.2. Velocity-Dependent Model

If the frictional contact force is modelled with a viscous behaviour (velocity formulation, which is similar to a viscous damper formulation), the frictional force will simply be as follows:

$$F_R(\dot{w}_{rel}) = c_T \, \dot{w}_{rel} \tag{53}$$

where c_T is the viscous damping constant. Unlike the Jenkins model, this model is always dissipative, even in the case of a pure stick cycle. Under the single harmonic assumption, the generic stick-slip cycle assumes a simplified expression for the force. In Figure 7, the nonlinear friction force against time and the hysteresis loop are depicted.

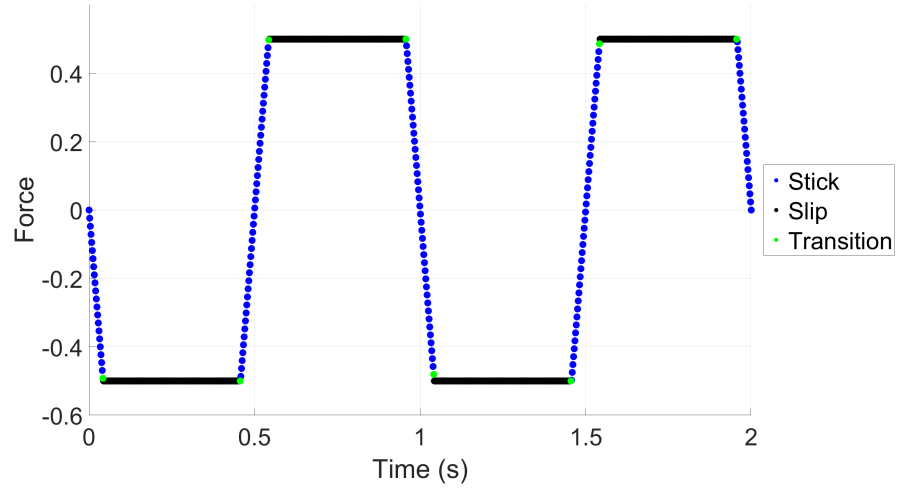

(a) Force against time

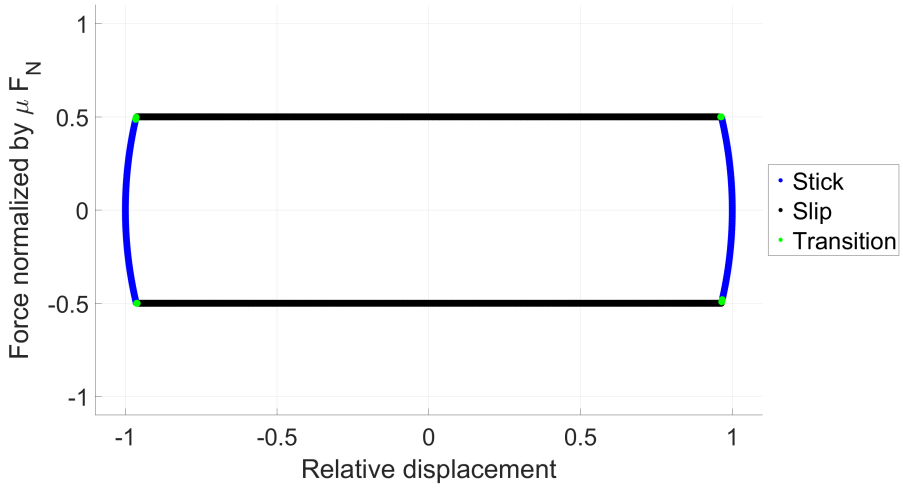

(b) Force against relative displacement.

Figure 7: Simplified velocity-dependent element under the single harmonic assumption.

If the value of $c_T \Omega a$ is lower than μF_N, the element will reduce to a dashpot of value c_T. If $c_T \Omega a$ exceeds μF_N, a stick-slip cycle will occur. From the hysteresis loop, it must be noticed that this friction element does not introduce any stiffness into the system. Moreover, in the generic case of a stick-slip cycle, the value of Δw_{slip} can also be derived as shown:

$$\Delta w_{slip} = \sqrt{a^2 - \left(\frac{\mu F_N}{c_T \Omega}\right)^2} \tag{54}$$

4.2. Modelling Methodology

A one-dimensional FE bar element is used to model the axial and torsional motion of the rod with frictional clamps. In this FE model, half of the rod with symmetric boundary conditions and Clamp B is used to represent the full model. The clamp is assumed to be only applied on the last node. A base excitation is used to excite the clamp, and the displacement of the clamp, $u_B(t)$, is prescribed with a certain frequency Ω.

One-dimensional Jenkins and velocity-dependent elements with constant normal load are used to compute the friction force [58]. F_N is the normal load; k_T is the tangential contact stiffness; c_T is the

viscous damping coefficient of the contact; μ is the friction coefficient. There are two contact statuses for these two elements, which are sticking and sliding. The description of these two elements can be referred to Section 4.1.

The equation of motion for the FE model with friction forces is given in Equation (55):

$$\underline{\underline{\mathbf{M}}}\,\ddot{\underline{U}}(t) \;+\; \underline{\underline{\mathbf{C}}}\,\dot{\underline{U}}(t) \;+\; \underline{\underline{\mathbf{K}}}\,\underline{U}(t) \;+F_F = 0 \tag{55}$$

where $\underline{\underline{\mathbf{M}}}$, $\underline{\underline{\mathbf{C}}}$ and $\underline{\underline{\mathbf{K}}}$ are the mass, viscous damping and stiffness matrices respectively. $\underline{U}(t)$ is the generalized displacement vector of the rod; $u_B(t)$ is the prescribed displacement of the left frictional clamp; F_F is the friction force. The classic AFTHB procedure is used to solve the Equation 55 in the frequency domain [62]. With the HBM, the numerical solutions is discretised into Fourier series truncated to a certain order N_h, and shown as in the equation below:

$$\underline{U}\,(t) = \sum_{h=0}^{Nh} Real\left\{e^{ih\omega t} \bullet \left(\underline{U}^{h,c} - \underline{U}^{h,s}i\right)\right\} \tag{56}$$

$$\underline{\tilde{U}} = \left[\underline{U}^{0,c},\;\; \underline{U}^{1,c} - \underline{U}^{1,s}i,\;\; \underline{U}^{h,c} - \underline{U}^{h,s}i\right]^T \tag{57}$$

Then, the equation of motion, which is originally formulated in the time domain (Equation (55)), can be rewritten in the frequency domain to yield the following expression.

$$\underline{\underline{\mathbf{A}}}\,\underline{\tilde{U}} + \;\tilde{F}_F\,(\tilde{u}_{71} \;- \tilde{u}_B) = 0 \tag{58}$$

Since the contact friction model is defined in the time domain as shown in Section 4.1, AFTHB procedure is used to compute the contact friction force in the time domain F_F and transfer that into frequency domain $\tilde{F}_F$ using the inverse discrete Fourier transformation (IFFT).

To obtain the dynamic response of the bar-clamp system for a range of excitation frequencies Ω, the classical predictor-corrector continuation technique is used to track the evolution of the results with respect to a certain chasing parameter. In this work, excitation frequency Ω is the chasing parameter. A secant predictor and pseudo-arc-length corrector are used [63].

5. Numerical Examples

5.1. Description of the Test Cases

For the axial vibration study, the dimension of the rod is given as a length of 70 mm, width of 14 mm and thickness of 4 mm. The material property of the rod is a density of 1400 kg/m^3, Young's modulus of 3.5 GPa and Poisson's ratio of 0.38. A one-dimensional finite element (FE) bar element is used. There are 71 nodes in total, with only one degree of freedom for each node to model the axial motion of the rod.

For the torsional vibration bar study, steel pipes with shrink fit is used to represent the case. The bar has a circular cross-section with a diameter of 7 mm, and the free length of the bar is 250 mm. The friction coefficient between the clamp and the bar is taken as 0.45. The material of the bar is taken as typical standard steel, which has the modulus of elasticity of 210 GPa, Poisson's ratio of 0.28 and density of 7800 kg/m^3. In terms of the numerical simulation, the only difference between the resultant loads of interest are the torsion moments, which also root from the contact friction as explained in Section 2.3.

5.2. Results:Model in Axial Motion

The analytical and numerical results presented within this study are nondimensionalised (frequency: $\tilde{\Omega}$, amplitude: α).

5.2.1. Jenkins Element

The two separate solutions of the axially vibrating bar with Jenkins friction approach for full-stick and full-slip regimes are shown in a representative plot in Figure 8 which corresponds to the case displayed in Figure 5c. Re-emphasising that the valid solutions are ones that result in lower amplitudes for the same excitation frequency. The most significant feature of this representative plot in Figure 8 is that the full-stick regime occurs around the resonance where the minima of the required frictional contact forces are located. The frequency interval, where full-stick is prevalent, can be expanded or shrunk depending on the maximum friction force or the amplitude of the clamp motion.

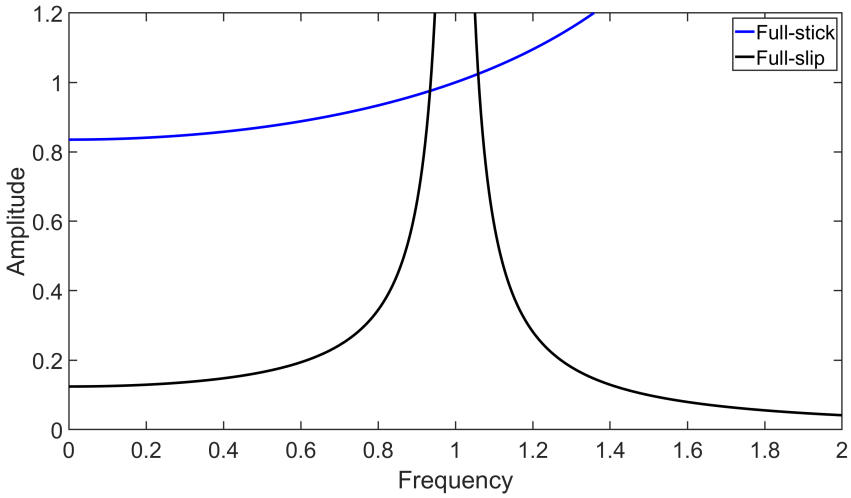

Figure 8: A sketch of the analytical solutions for bar in axial motion with Jenkins model.

Figure 9 shows the analytical and numerical results together for the axially excited rod with the Jenkins friction approach, which assumes $\tilde{k}_T = 2.5$. Both analytical and numerical results display the same behaviour with some considerable level of accuracy. The analytical model predicts lower vibration amplitudes compared to the numerical model in the pre-resonance slip region. In the post-resonance slip region, however, analytical values are slightly greater than the results of the numerical analysis. This is mainly caused by the representation of the friction forces by a simpler harmonic function which affects the dissipation characteristics leading to these differences in the predicted amplitudes. The gap between these two models is closed towards the resonance and becomes almost negligible in the stick regime. The only difference is the numerical model predicts a small peak just before going back to sliding. The analytical model does not show that curvature before the peak, but both models predict the maximum amplitude with good precision. In the end, it can be stated that the results of both analytical and numerical models show good agreement.

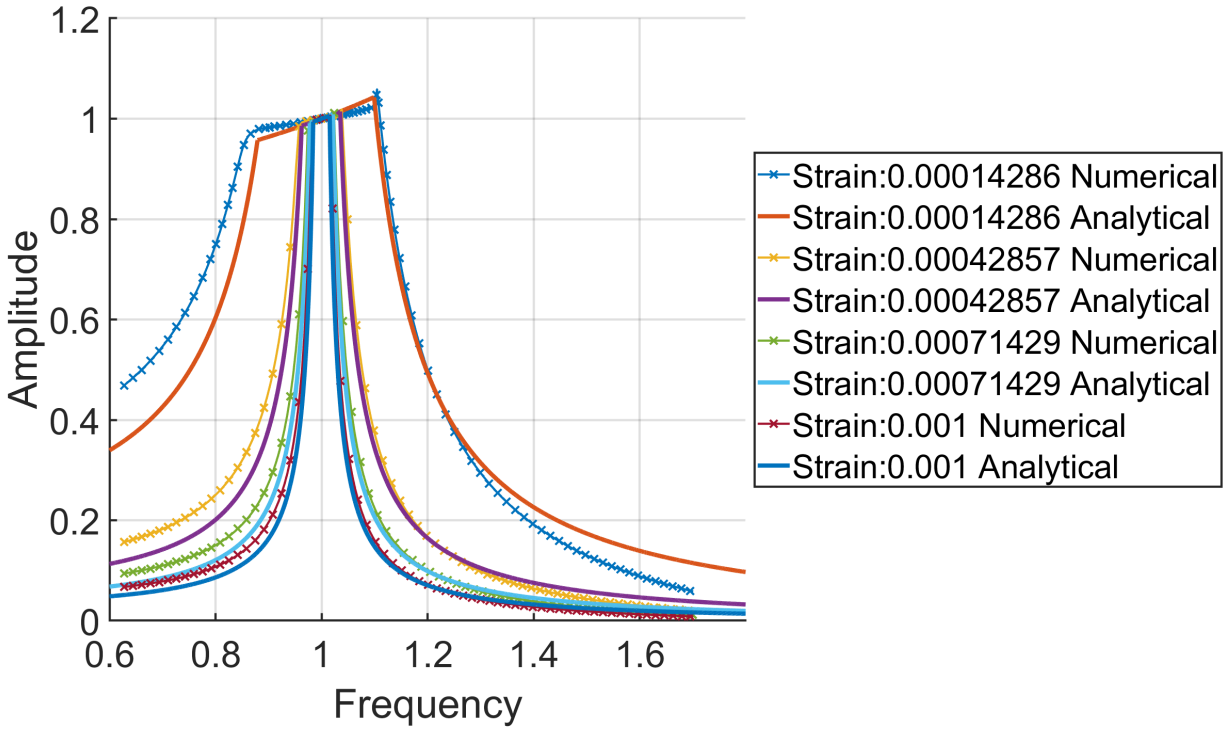

Figure 9: Comparison of analytical and numerical results for the axial case with Jenkins model.

Referring to the same figure (Figure 9), under constant normal load, increasing the clamp motion amplitude, which is expressed as W_A/L ratio, shrinks the full-stick regime dominance within the selected frequency interval, in other words, the slip region expands eventually causing more friction damping. The maximum amplitude is located towards the end of the post-resonance full-stick regime exceeding the clamp motion amplitude. This can be explained by the presence of the contact stiffness, which also controls the slope of the stick regime. The total stiffness of the system does not only consist of the stiffness of the bar, and the system is not directly excited with a simple harmonic force. The moving clamp interacts with the bar over the contact, which is described with a Jenkins element for this case. Hence, the amplitude of the bar may go slightly beyond the amplitude of the clamp motion. The small peak at the end of the stick region also occurs for the same reason.

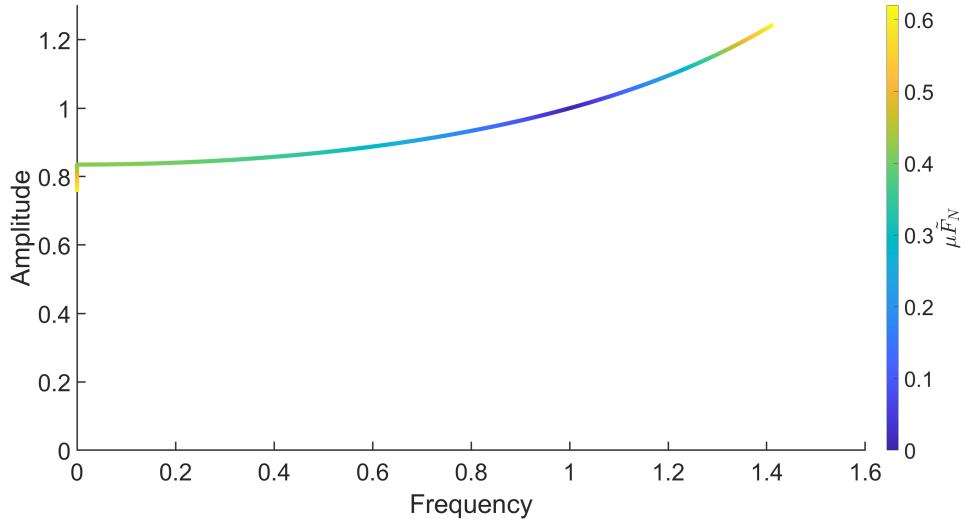

(a) $\tilde{k}_T = 2.5$

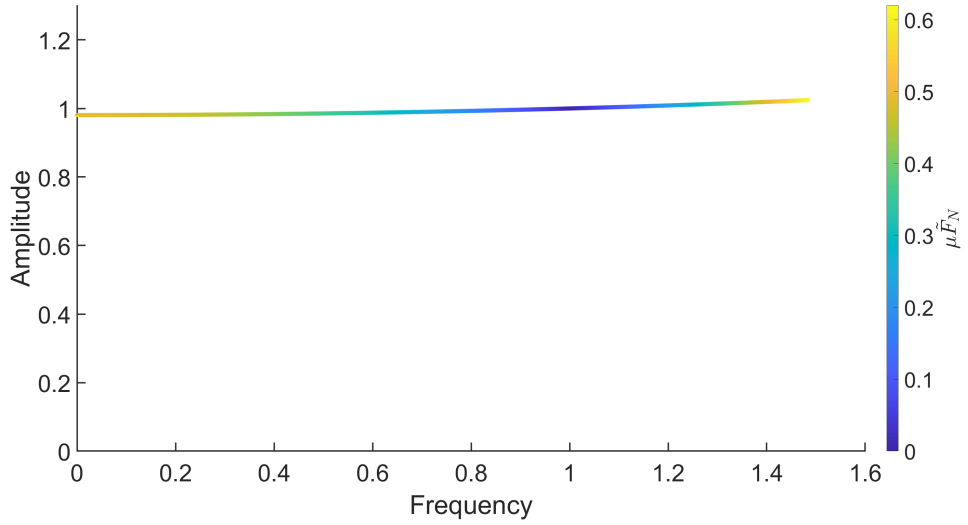

(b) $\tilde{k}_T = 25.3$

Figure 10: Expansion of the stick limit boundaries with $\mu\tilde{F}_N$. Limit amplitude against limit frequency for different values of $\tilde{k}_T$ under the constat clamp motion amplitude of 0.0001.

Figure 10 displays the limit frequency and amplitudes values of the full-stick region depending on the maximum friction force, $\mu\tilde{F}_N$ with various contact stiffness coefficients $\tilde{k}_T$ under the same clamp motion amplitude. The first thing to note is that the stick region expands with increasing maximum friction force, $\mu\tilde{F}_N$. This expansion is greater in pre-resonance frequencies and less in the post-resonance region. For lower $\tilde{k}_T$ values, the curve has a greater slope and thus, the limit amplitudes pass beyond the value 1, which is the amplitude of the clamp motion. Meanwhile, increasing the tangential contact stiffness reduces the slope and leads to a flatter, full-stick region. This can be explained by the contact stiffness values considered to be greater than the bar's axial stiffness. Rising $\tilde{k}_T$ widens the gap between these stiffnesses and hinders the dynamic interaction of the contact. Thus, the overall behaviour of the system becomes more bar dominated. The curves become flatter, and the interval of amplitude values, that approach closer to 1, is extended.

The stick limits shown in Figure 11 plotted based on Equation (24), shows the minimum necessary limit frictional force, $\mu\tilde{F}_N$, under constant clamp motion amplitude. Based on this visualised data, the

first thing to notice is that the minimum necessary limit friction force becomes zero at the resonance frequency. This is an expected result for a system with no damping source which is always present, in other words, independent of stick and slip regimes of the contact friction. The only source of damping of this system is the frictional contact, which behaves elastically in a full-stick regime. Considering that this plot marks the border of a damped (full-slip) and an undamped (full-stick) regime, a purely conservative elastic dynamic behaviour can be understood. Moreover, in the static case where $\tilde{\Omega} = 0$, the minimum necessary limit frictional force has a finite value, and it decreases towards the resonance frequency, reaching zero at the resonance as mentioned earlier. From the resonant frequency towards higher frequencies, the least necessary limit frictional force increases. Besides, in the pre-resonant region, the least necessary limit frictional force increases if the contact stiffness $\tilde{k}_t$ is increased. On the other hand, in the post-resonant frequencies, the minimum necessary friction force this trend is reversed.

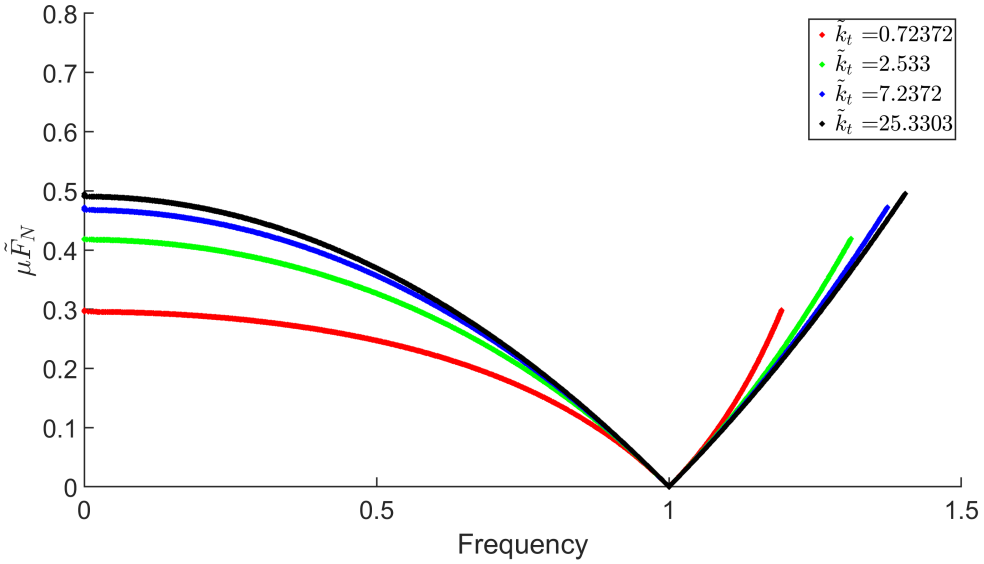

Figure 11: The least necessary $\mu\tilde{F}_N$ for full-stick regime in axial Jenkins model.

5.2.2. Velocity-Dependent Element

The same case of the axially vibrating bar under the excitation of moving frictional clamps is modelled with the velocity-dependent model.

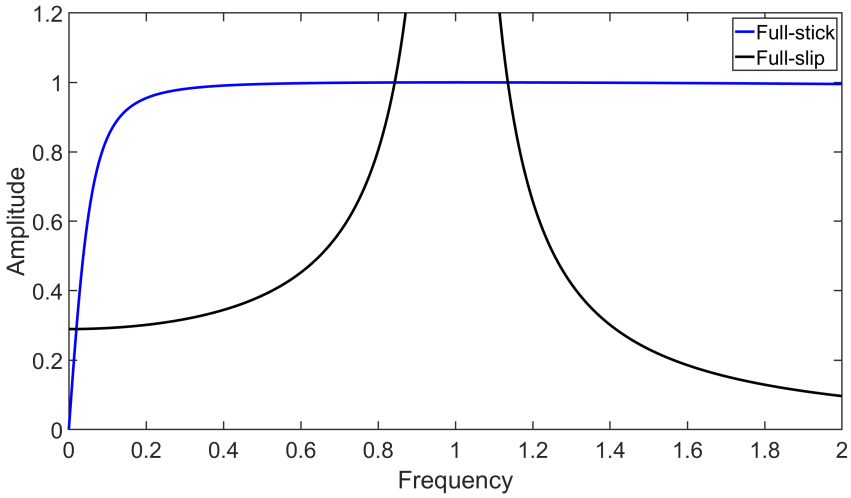

Figure 12: A sketch of the analytical solutions for bar in axial motion with velocity-dependent model.

Again, the solution procedure divides the motion into two regimes depending on the existence of slip at the contact interface between the bar and the clamp, like the model with Jenkins. The only difference is the calculation method of the friction force. A representative plot including the two contact conditions, stick and slip is presented in Figure 12. A noticeable aspect in this plot is that there is a tiny region for very low frequencies (around $\tilde{\Omega} = 0$) where clamps stick to the bar. Following this small stick region is a slip region with increasing frequency until the main stick region is located around the resonance. The amplitudes are almost fixed to the value of 1 in this second stick region. Therefore, it appears as a flat top in the plot. The second stick region is succeeded by another region dominated by the slip regime, which is similar to the case with the Jenkins model. Altogether, two regimes appear in two regions each. Thus, the solution consists of four regions.

To compare the results of the numerical and analytical approaches, Figure 13 is presented. The calculations to generate this plot $\tilde{c}_T$ is taken as 7.7. Overall, the results of both methods are in good agreement. The amplitudes that the analytical model predict are slightly smaller than the numerical predictions in the pre-resonance slip region. Later in the stick region around the resonance, the results agree almost perfectly. The amplitudes become 1 in the stick regime and remain constant throughout the region. In the post-resonance slip regime, the results start out very similar. However, with increasing excitation frequency, the results of the numerical model become smaller than their analytical correspondents. Since these trends are very similar to the Jenkins model, the reasons are expected to be the same, namely the error in damping caused by the representation of the contact forces in the slip regime.

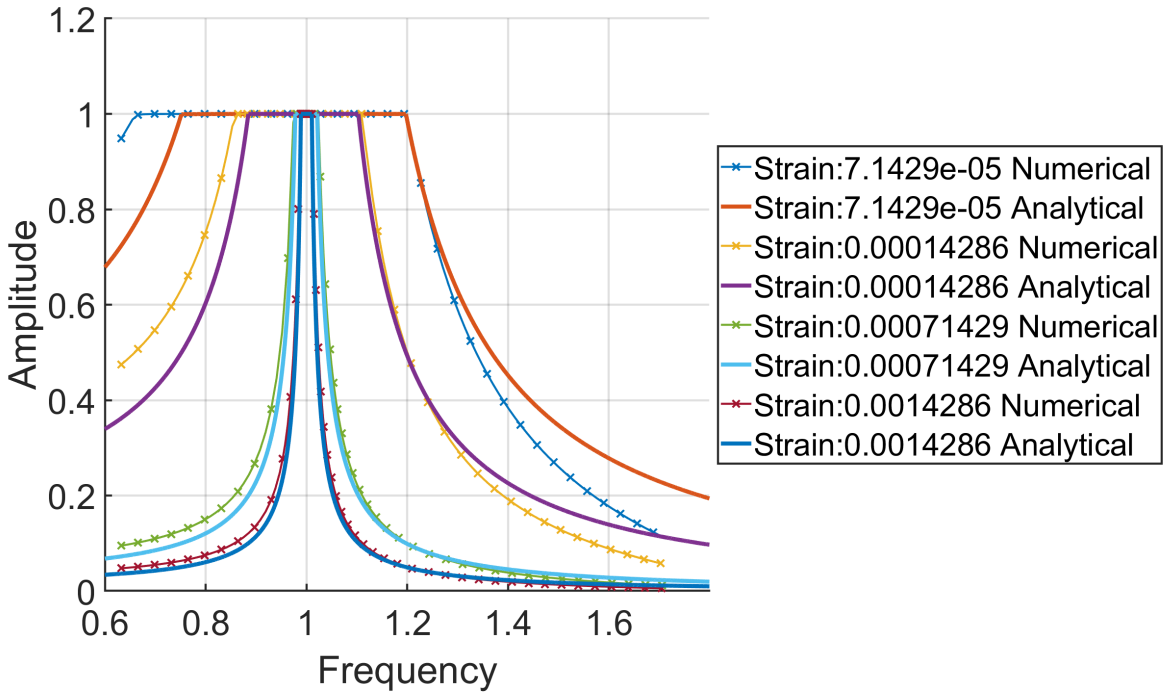

Figure 13: Comparison of analytical and numerical results for the axial case with velocity-dependent model.

Apart from these, Figure 13 points out that increasing clamp motion amplitude again shrinks the full-stick region. This is because increasing the clamp motion amplitude leads to greater required frictional contact forces. The friction forces attain the maximum value in larger intervals of frequency.

To understand the effect of the maximum frictional force on the limits of the stick regime, Figure 14 shows various $\tilde{c}_T$ values. For $\tilde{c}_T = 1.3$ (Figure 14a), an amplitude peak, which reaches its maximum value of $\alpha = 1$, which is visible at the resonance frequency. The rest of the amplitude values are slightly below 1 for pre-and post-resonant frequencies. The curve in the pre-resonant region rise up to 1 with a smaller gradient compared to the absolute value of the gradient of the falling amplitudes in the post-resonant region. Besides, the plots also show that greater $\tilde{c}_T$ values make the amplitude curve flatter equating all the values practically to 1.

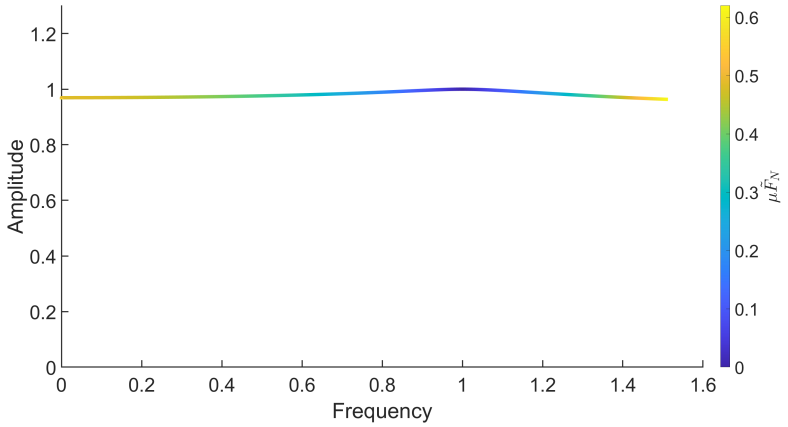

(a) $\tilde{c}_T = 1.3$

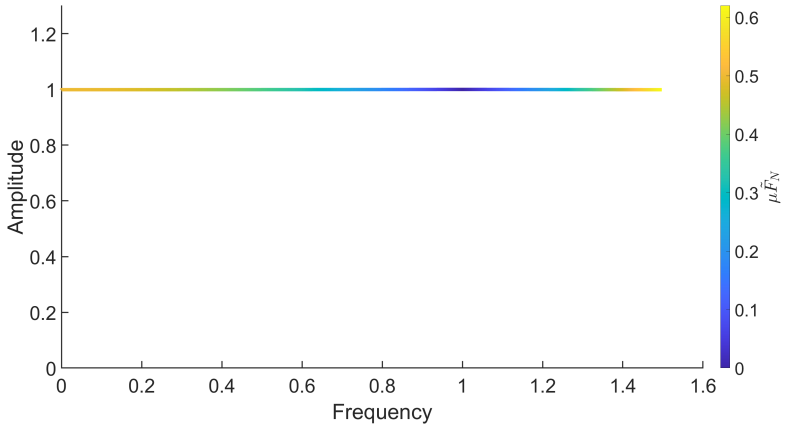

(b) $\tilde{c}_T = 7.7$

Figure 14: Enlargement of the stick limit boundaries with $\mu\tilde{F}_N$. Limit amplitude against limit frequency for different values of $\tilde{c}_T$ under the constat clamp motion amplitude of 0.0001.

In Figure 15 the least necessary frictional force is visualised using Equation (29) for this velocity-dependent model. The characteristics of the plots are pretty much the same, which could be expected. This figure again points out the limits of the conservative and dissipative regimes that are purely dependent on the status of the frictional contact. The condition that ends one regime and starts the other is precisely the same as the Jenkins model. The difference in this model is the approach which the dissipative regime is formulated. The curves are shaped dominantly by the conservative elastic regime and the condition that separates them from the full-slip regime.

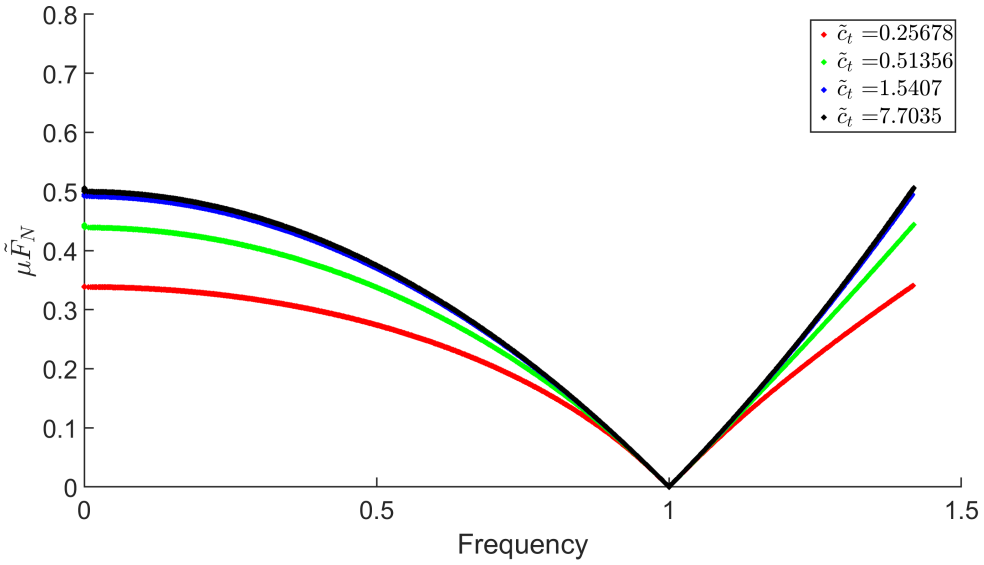

Figure 15: The least necessary $\mu\tilde{F}_N$ for full-stick regime in the velocity-dependent model.

5.3. Results:Model in Torsional Motion

5.3.1. Jenkins Element

Like the axial model, for the torsional bar model subjected to friction employing the Jenkins approach, the analytical solution is performed by decomposing the dynamics of the system in two regimes based on the contact conditions. The solutions of the stick and slip regimes are schematically shown in Figure 16. Following the same methodology, the valid solution is the one that provides the lower amplitude.

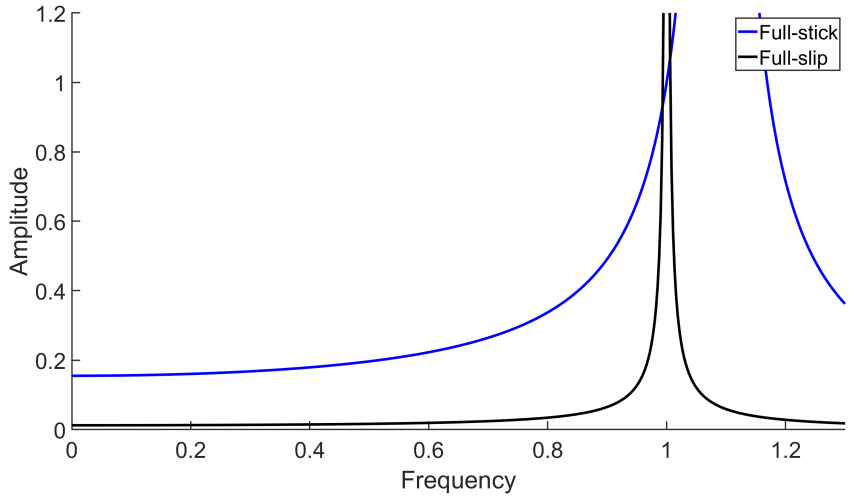

Figure 16: A sketch of the analytical solutions for bar in torsional motion with Jenkins model.

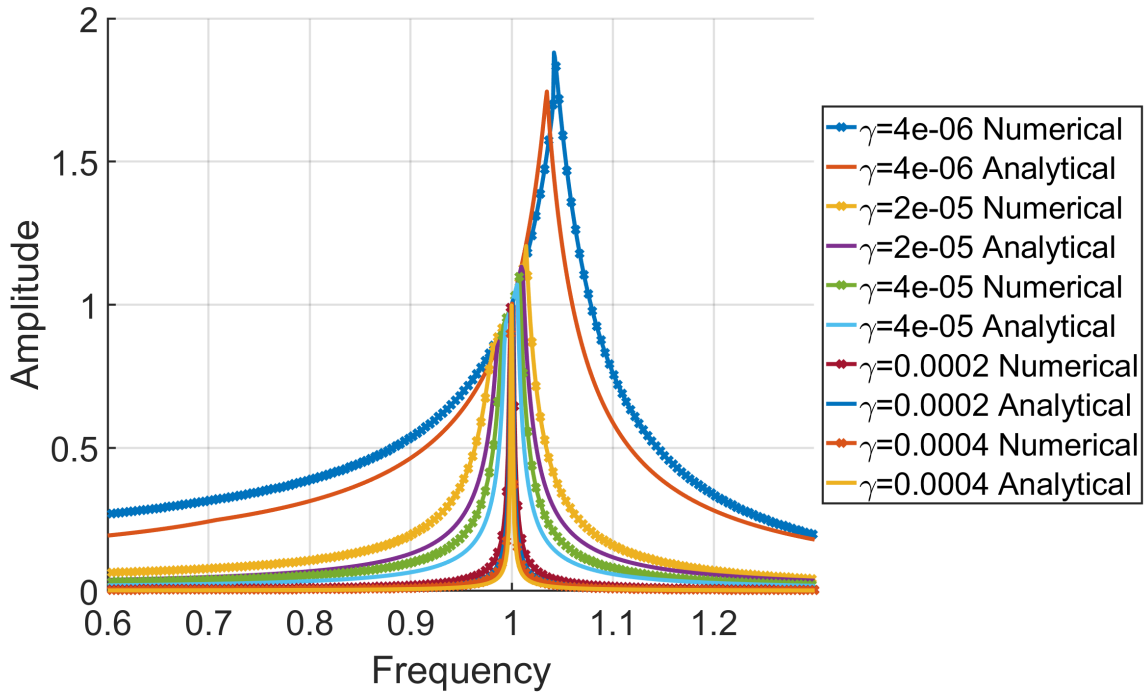

Figure 17: Comparison of analytical and numerical results for the torsional case with Jenkins model.

The results of the bar model with a circular cross-section fitted into a pipe, which is described in detail earlier, are visualised in Figure 17 while keeping $\tilde{k}_T = 0.9$ slightly softer than the axial case. The clamp motion amplitudes are defined over rotation per unit length, γ this time. All the comments made for the axial model are valid for this torsional model as well, such as the expansion of the stick region with falling γ values and the differences between the analytical and numerical models. This is the consequence of the same characteristics of the governing equations. However, in the curve that is excited with the lowest γ, one can quickly notice that the stick region is dominant from the start of the frequency interval of interest ($\tilde{\Omega} = 0.6$) until the beginning of the post-resonance slip regime which is around $\tilde{\Omega} = 1.07$. This is an example of the case described in Figure 5b. Here, the selected contact stiffness values are smaller than the ones in the axial model and closer to the bar stiffness. Therefore, the amplitude values tend to go further beyond 1, which is caused by more interaction of the contact and the bar. The curve plotted for the smallest clamp motion amplitude almost reaches 2.

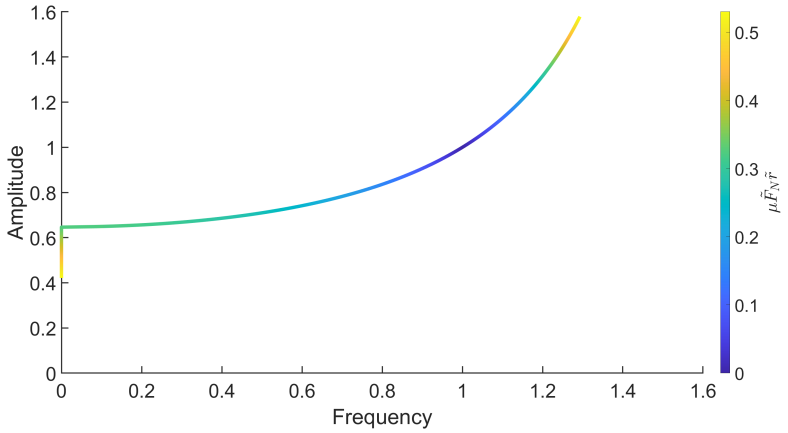

(a) $\tilde{k}_T = 0.9$

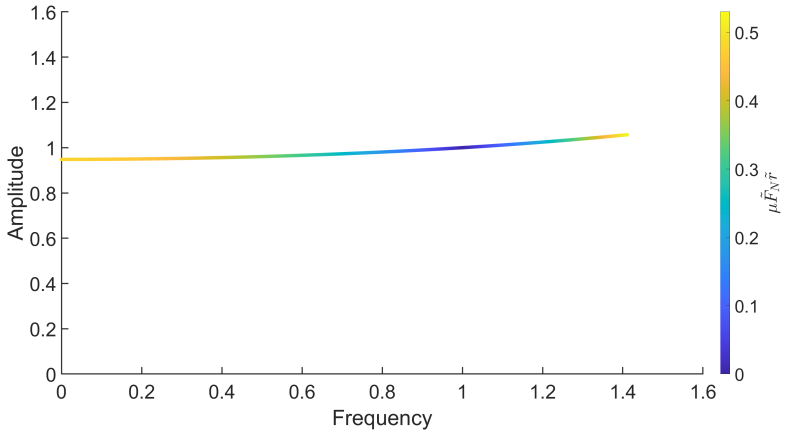

(b) $\tilde{k}_T = 9.2$

Figure 18: Growth of the stick limit boundaries with $\mu\tilde{F}_N$. Limit amplitude against limit frequency for different values of $\tilde{k}_T$ under the constat clamp motion amplitude of 0.001.

Figure 18 facilitates exploring the influence of the contact stiffness on the growth of the stick region for the torsional bar with the Jenkins friction approach. Again, the stick region expands easier in the pre-resonant region towards smaller frequencies compared to the growth in the post-resonant frequencies. Considering that the contact is softer than the axial model, the curves have greater gradients and consequently, rise to greater amplitude values. Stiffening the contact flattens the amplitude curve just as in the axial model.

Like the axial case with the Jenkins element, the minimum necessary frictional moment for a full-stick regime is displayed in Figure 19 using Equation (41). Knowing that the system characteristics of the torsional model with the Jenkins element are precisely the same as the axial model with the Jenkins element, one can explain this figure using the same perspective.

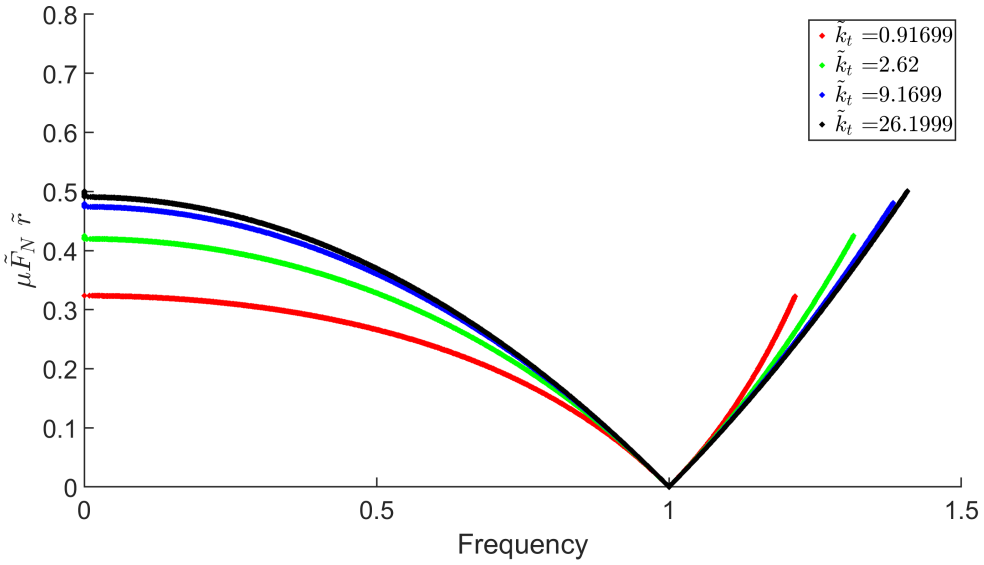

Figure 19: The least necessary $\mu\tilde{F}_N\ \tilde{r}$ for full-stick regime in torsional Jenkins model.

5.3.2. Velocity-Dependent Element

The results of the final analytical model built within the scope of this study are acquired by merging the two separate solutions as done in the previous models. These separate solutions, which belong to the regimes of stick and slip contact conditions, are sketched in Figure 20. This sketch exhibits four regions of stick and slip identical to the axial model with a velocity-dependent friction approach. This is a natural consequence of closely related characteristics of the governing equations.

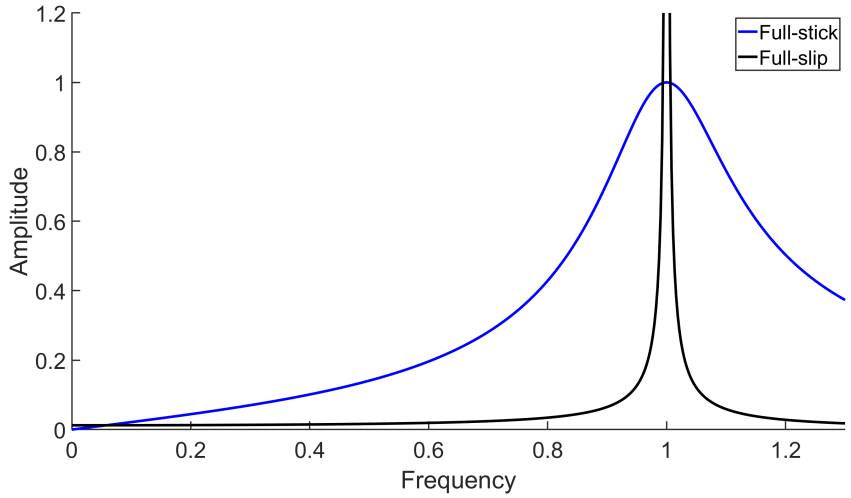

Figure 20: A sketch of the analytical solutions for bar in torsional motion with velocity-dependent model.

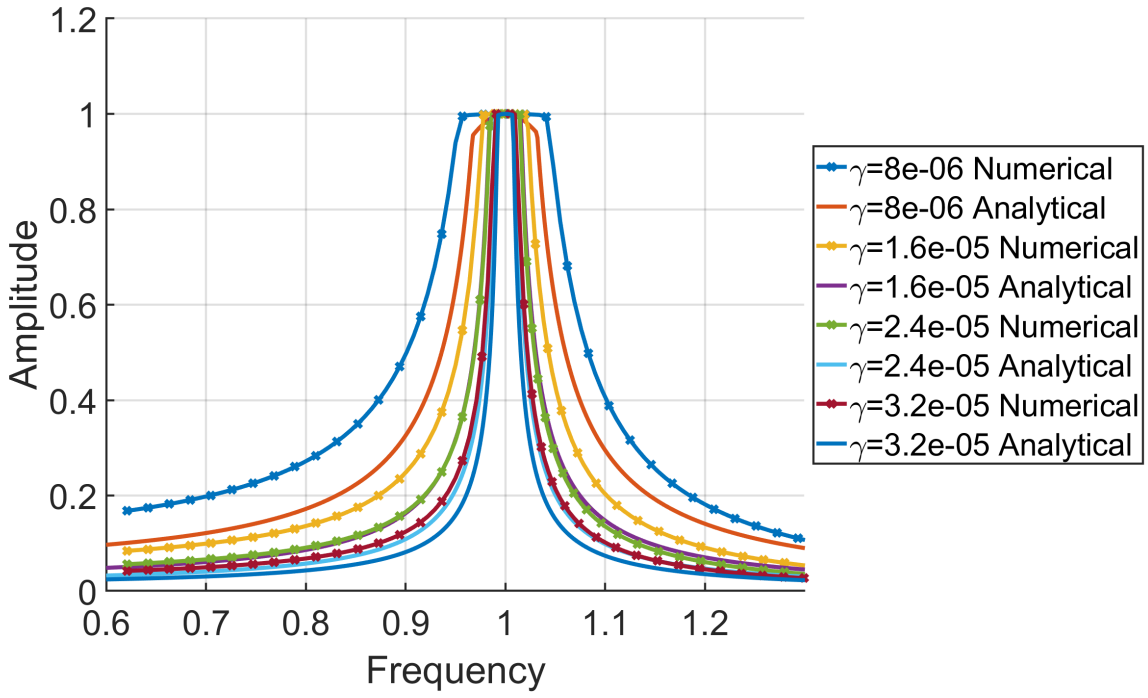

Figure 21: Comparison of analytical and numerical results for the torsional case with velocity-dependent model.

The results produced utilising the analytical and numerical models for a range of various clamp displacement amplitudes are presented in Figure 21. Here, $\tilde{c}_T$ is kept constant and selected as 0.1, which is very small compared to the examples of the axial case. Throughout the whole interval of frequencies of interest, both numerical and analytical solutions show very similar behaviours. However, the analytical solution predicts a motion with slightly less amplitude except for the frequency of resonance, where both are equal to 1. The numerical approach suggests that the stick regime is almost a flat-top region around the resonance, whereas the analytical method yields a curve with a greater curvature which depends on $\tilde{c}_T$. The margin of error in both stick and slip regimes (in stick more dramatically) drops as the clamp motion amplitude increases. Comparing these results to the axial case, another factor that affects the gap between the numerical and analytical approaches is the $\tilde{c}_T$, the damping coefficient of the contact, which controls the curvature of the plot in the stick regime. These models are in better agreement in the full-stick regimes for greater values of parameter $\tilde{c}_T$. As the $\tilde{c}_T$ rises, the amplitude response of the stick regime becomes flatter and the values closer to the boundaries of the slip regime climb closer to 1. This behaviour can be seen in Figure 22 (22a and 22b), which visualise the effects of $\mu\tilde{F}_N$ and $\tilde{c}_T$ on the boundaries of the stick and slip regions. Figure 22 also shows that the expansion of the stick region is easier towards smaller frequencies compared to growth in the positive direction along the axis of frequency.

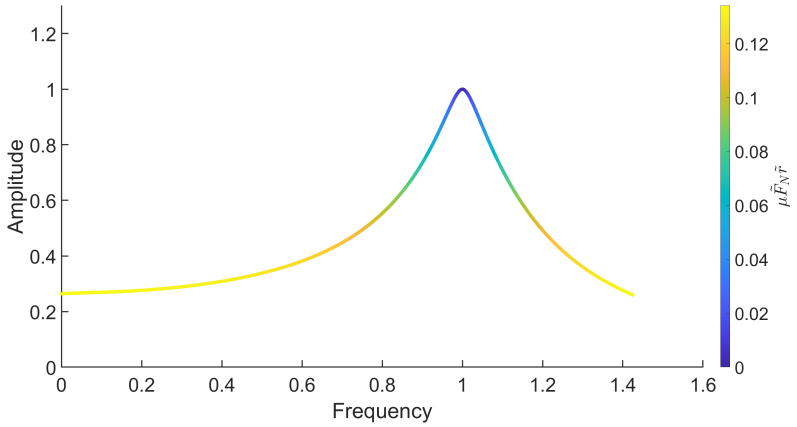

(a) $\tilde{c}_T = 0.1$

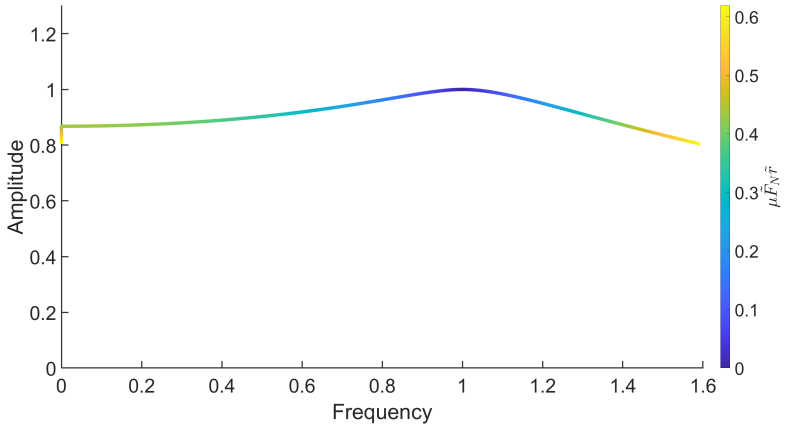

(b) $\tilde{c}_T = 0.8$

Figure 22: Enlargement of the stick limit boundaries with $\mu\tilde{F}_N$. Limit amplitude against limit frequency for different values of $\tilde{c}_T$ under the constat clamp motion amplitude of 0.001.

Finally, Figure 23 displays the relationship with the minimum required frictional moment for a full-stick regime based on Equation (41). Comparing this in every aspect, one can conclude that the plots are very similar to the ones presented in Section 5.2.2 and therefore, the interpretation must be made using the same approach.

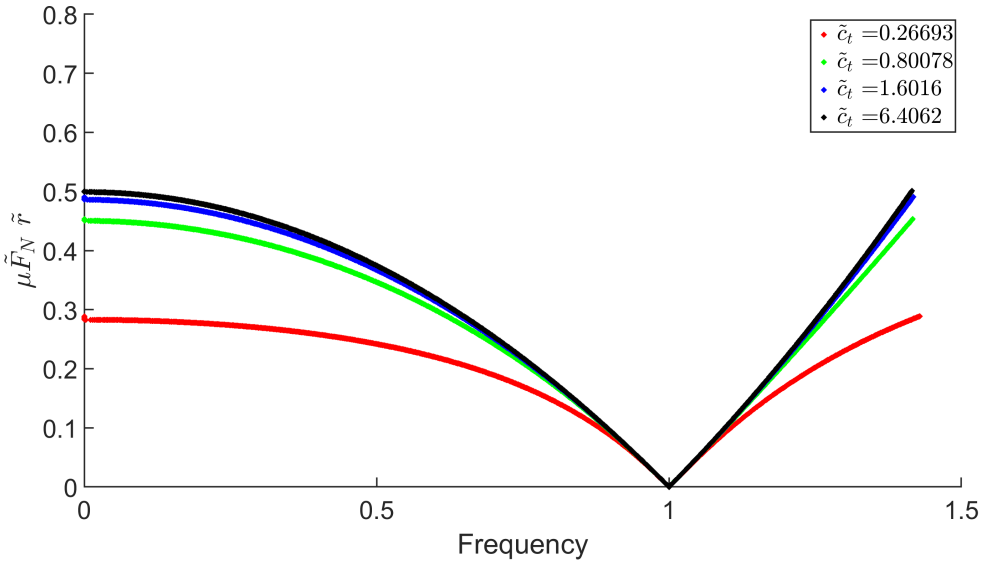

Figure 23: The least necessary $\mu\tilde{F}_N\ \tilde{r}$ for full-stick regime in torsional velocity-dependent model.

6. Conclusion

This study presents a new analytical solution to predict the steady-state forced vibration response of bars with frictional clamps under the axial and torsional motion. The principle of the new solution consists in using the Dirac delta function to describe the modeling of nonlinear clamps into the concentrated nonlinear loads due to the friction. In this study, the nonlinear loads caused by the friction are modelled using two different models, namely, Jenkins and velocity-dependent models to describe the full-stick and full-slip regime. The equations of motion including the friction models are then nondimensionalised and solved by using the Galerkin method to obtain the response of each regime separately. The final solution for the dynamical response of the bar-clamp system can be then found by combining the solutions of both regimes. The performance of the proposed analytical solution was demonstrated by two numerical examples. To validate the proposed analytical solution, a well known numerical method based on harmonic balance methods that requires fewer simplifications/assumptions is performed as the reference. The results of the numerical and analytical models are compared with each other and are overall found to be in good agreement.

The results of both Jenkins and velocity-dependent models show that the stick regime governs the behaviour around the resonance since the necessary excitation forces reach their minima at the resonance. The interval where stick regime is dominant is controlled by the maximum friction forces. The greater the maximum friction forces are, the larger the stick regime interval. Likewise, increasing the prescribed clamp motion amplitude shrinks the stick region. Here, the maximum friction forces are constant, but the required frictional forces climb. The displacement amplitude of bars with the Jenkins friction model exceeds the imposed clamp motion amplitude. The main reason is the interaction of the contact stiffness with the bar. The interaction becomes more significant if the contact stiffness is closer to the bar stiffness, and thus, the overshoot of the amplitude becomes greater. For stiffer contacts, the overshoot becomes negligible, and the plot of the stick region becomes a flat line fixed at the amplitude value of 1. The bar-clamp system built by using the velocity-dependent model generally shows similar behaviour. However, the peak amplitude value never exceeds unity in this model. The stick regime may be found at two different locations, at very small frequencies, as well as around the resonance. The stick regime around the resonant frequency looks almost like a flat top for a larger contact damping coefficient and has a considerably significant curvature for the lower contact damping.

In summary, the following conclusions can be drawn from this study:

- The study introduces a novel analytical solution for predicting the dynamic behaviour of bars with frictional clamps, incorporating the Dirac delta function to model concentrated nonlinear loads due to friction.
- It employs both Jenkins and velocity-dependent friction models to comprehensively understand the full spectrum of stick-slip behaviour in bar-clamp systems.
- The proposed analytical solution is validated through a comparative analysis with a standardised numerical method based on harmonic balance, demonstrating its accuracy and reliability.
- The research provides significant understanding of the effects of friction forces and contact stiffness on the vibrational response of the system, that can help the design and optimisation of mechanical systems.

Acknowledgement

Mertol Tüfekci would like to acknowledge the support of the Scientific and Technological Research Council of Turkey (TUBITAK) (fund BİDEB 2213 2016/2) that makes this research possible. Yekai Sun is grateful to China Scholarship Council (File NO. 201708060239) for providing the financial support.

The authors would like to thank Alessandra Vizzaccaro for her valuable contributions to this research.

The authors would also like to acknowledge computational resources and support provided by the Imperial College Research Computing Service (http://doi.org/10.14469/hpc/2232).

References

[1] Ö. E. Genel, M. Tüfekci, E. Tüfekci, Free vibrations of spatial frame structures: Analytical modelling and solution, Journal of Vibration and Control 29 (2023) 4492–4502. URL: http://journals.sagepub.com/doi/10.1177/10775463221122086. doi:10.1177/10775463221122086.

[2] Şeref D. Albas, H. Ersoy, B. Akgöz, Ömer Civalek, Dynamic analysis of a fiber-reinforced composite beam under a moving load by the ritz method, Mathematics 9 (2021). doi:10.3390/math9091048.

[3] H. Koc, E. Tufekci, A novel approach of bending behavior of carbon nanotubes by combining the effects of higher-order boundary conditions and coupling through doublet mechanics, Mechanics of Advanced Materials and Structures (2023). doi:10.1080/15376494.2023.2263767.

[4] U. Eroglu, E. Tufekci, Small-Amplitude free vibrations of straight beams subjected to large displacements and rotation, Applied Mathematical Modelling 53 (2018) 223–241. doi:10.1016/j.apm.2017.08.028.

[5] E. Tufekci, Exact Solution of Free in-Plane Vibration of Shallow Circular Arches, International Journal of Structural Stability and Dynamics 01 (2001) 409–428. doi:10.1142/s0219455401000226.

[6] A. Yucel, A. Arpaci, E. Tufekci, Coupled axial-flexural-torsional vibration of Timoshenko frames, JVC/Journal of Vibration and Control 20 (2014) 2366–2377. doi:10.1177/1077546313484348.

[7] K. Senthil Kumar, I. Siva, P. Jeyaraj, J. Winowlin Jappes, S. Amico, N. Rajini, Synergy of fiber length and content on free vibration and damping behavior of natural fiber reinforced polyester composite beams, Materials & Design (1980-2015) 56 (2014) 379–386. URL: http://dx.doi.org/10.1016/j.matdes.2013.11.039https://linkinghub.elsevier.com/retrieve/pii/S0261306913010881. doi:10.1016/j.matdes.2013.11.039.

[8] S. H. Crandall, The role of damping in vibration theory, Journal of Sound and Vibration 11 (1970) 3–18. doi:10.1016/S0022-460X(70)80105-5.

[9] B. Feeny, A. Guran, N. Hinrichs, K. Popp, A Historical Review on Dry Friction and Stick-Slip Phenomena, Applied Mechanics Reviews 51 (1998) 321–341. URL: https://asmedigitalcollection.asme.org/appliedmechanicsreviews/article/51/5/321/401371/A-Historical-Review-on-Dry-Friction-and-StickSlip. doi:10.1115/1.3099008.

[10] M. Brake, The Mechanics of Jointed Structures: Recent Research and Open Challenges for Developing Predictive Models for Structural Dynamics, 2018. doi:10.1007/978-3-319-56818-8.

[11] Y. Mabuchi, T. Hanazato, M. Watabe, Static shear friction tests on the model marble columns of the Parthenon for the aseismic retrofitting, Transactions on the Built Environment 4 (1993) 475–482. URL: https://www.witpress.com/elibrary/wit-transactions-on-the-built-environment/4/13587. doi:10.2495/STR930461.

[12] I. N. Psycharis, J. V. Lemos, D. Y. Papastamatiou, C. Zambas, C. Papantonopoulos, Numerical study of the seismic behaviour of a part of the Parthenon Pronaos, Earthquake Engineering & Structural Dynamics 32 (2003) 2063–2084. URL: https://onlinelibrary.wiley.com/doi/abs/10.1002/eqe.315?casa_token=Et9vCVFGlB8AAAAA:oxvg1Cf1nmutjjh_VbRogqCdilIRdjm8nN0UYVLwKQFKaViL0kZ4fph1c2DiUdqeGw7e5SDgapBvL5Uhttps://onlinelibrary.wiley.com/doi/abs/10.1002/eqe.315?casa%7B%5C_%7Dtoken=Et9vCVFGlB8AAAA. doi:10.1002/eqe.315.

[13] M. Ferris, F. Tin-Loi, Limit analysis of frictional block assemblies as a mathematical program with complementarity constraints, International Journal of Mechanical Sciences 43 (2001) 209–224. URL: https://linkinghub.elsevier.com/retrieve/pii/S0020740399001113. doi:10.1016/S0020-7403(99)00111-3.

[14] J. Esteban, C. A. Rogers, Energy dissipation through joints: theory and experiments, Computers & Structures 75 (2000) 347–359. URL: https://www.sciencedirect.com/science/article/pii/S0045794999000966. doi:https://doi.org/10.1016/S0045-7949(99)00096-6.

[15] L. Gagnon, M. Morandini, G. L. Ghiringhelli, A review of friction damping modeling and testing, Archive of Applied Mechanics 90 (2020) 107–126. URL: https://doi.org/10.1007/s00419-019-01600-6. doi:10.1007/s00419-019-01600-6.

[16] P. Barlek, D. Ambrosini, B. Luccioni, Generalized friction panel: An innovative passive energy dissipation device for structures subjected to seismic loading, Engineering Structures 283 (2023) 115898. URL: https://www.sciencedirect.com/science/article/pii/S0141029623003127. doi:https://doi.org/10.1016/j.engstruct.2023.115898.

[17] D. Karnopp, Computer Simulation of Stick-Slip Friction in Mechanical Dynamic Systems, Journal of Dynamic Systems, Measurement, and Control 107 (1985) 100–103. URL: https://doi.org/10.1115/1.3140698. doi:10.1115/1.3140698. arXiv:https://asmedigitalcollection.asme.org/dynamicsystems/article-pdf/107/1/100/5492329/100_1.pdf.

[18] L. Couch, F. M. Tehrani, A. Naghshineh, R. Frazao, Shake table response of a dual system with inline friction damper, Engineering Structures 281 (2023) 115776. URL: https://www.sciencedirect.com/science/article/pii/S0141029623001906. doi:https://doi.org/10.1016/j.engstruct.2023.115776.

[19] Q. Xie, Y. Liu, B. Zhang, Y. Wu, F. Hu, Seismic performance of glulam frame with friction damper and column shoe: Experimental investigation and simplified numerical model, Engineering Structures 298 (2024) 117036. URL: https://www.sciencedirect.com/science/article/pii/S0141029623014517. doi:https://doi.org/10.1016/j.engstruct.2023.117036.

[20] S. W. Shaw, On the dynamic response of a system with dry friction, Journal of Sound and Vibration 108 (1986) 305–325. doi:10.1016/S0022-460X(86)80058-X.

[21] Y. J. Ahn, J. Barber, Response of frictional receding contact problems to cyclic loading, International Journal of Mechanical Sciences 50 (2008) 1519–1525. URL: https://linkinghub.elsevier.com/retrieve/pii/S0020740308001203. doi:10.1016/j.ijmecsci.2008.08.003.

[22] S. Natsiavas, Analytical Modeling of Discrete Mechanical Systems Involving Contact, Impact, and Friction, Applied Mechanics Reviews 71 (2019). doi:10.1115/1.4044549.

[23] R. A. Ibrahim, Friction-induced vibration, chatter, squeal, and chaos part I: Mechanics of contact and friction, 1994. doi:10.1115/1.3111079.

[24] E. J. E. J. Berger, Friction modeling for dynamic system simulation, Applied Mechanics Reviews 55 (2002) 535. doi:10.1115/1.1501080.

[25] J. J. Sinou, O. Dereure, G. B. Mazet, F. Thouverez, L. Jezequel, Friction-induced vibration for an aircraft brake system - Part 1: Experimental approach and stability analysis, 2006. doi:10.1016/j.ijmecsci.2005.12.002.

[26] E. Pennestrì, V. Rossi, P. Salvini, P. P. Valentini, Review and comparison of dry friction force models, Nonlinear Dynamics 83 (2016) 1785–1801. doi:10.1007/s11071-015-2485-3.

[27] F. Marín, F. Alhama, J. Moreno, Modelling of stick-slip behaviour with different hypotheses on friction forces, International Journal of Engineering Science 60 (2012) 13–24. URL: https://linkinghub.elsevier.com/retrieve/pii/S002072251200122X. doi:10.1016/j.ijengsci.2012.06.002.

[28] I. R. Ionescu, J.-C. Paumier, On the contact problem with slip displacement dependent friction in elastostatics, International Journal of Engineering Science 34 (1996) 471–491. URL: https://linkinghub.elsevier.com/retrieve/pii/0020722595001093. doi:10.1016/0020-7225(95)00109-3.

[29] L. Xu, M. W. Lu, Q. Cao, Nonlinear vibrations of dynamical systems with a general form of piecewise-linear viscous damping by incremental harmonic balance method, Physics Letters A 301 (2002) 65–73. URL: http://linkinghub.elsevier.com/retrieve/pii/S037596010200960X. doi:10.1016/S0375-9601(02)00960-X.

[30] X. Tan, R. J. Rogers, Equivalent viscous damping models of coulomb friction in multi-degree-of-freedom vibration systems, Journal of Sound and Vibration 185 (1995) 33–50. doi:10.1006/jsvi.1994.0362.

[31] C. Leech, The modelling of friction in polymer fibre ropes, International Journal of Mechanical Sciences 44 (2002) 621–643. URL: https://linkinghub.elsevier.com/retrieve/pii/S0020740301000959. doi:10.1016/S0020-7403(01)00095-9.

[32] B. Kang, C. A. Tan, Nonlinear response of a beam under distributed moving contact load, Communications in Nonlinear Science and Numerical Simulation 11 (2006) 203–232. doi:10.1016/j.cnsns.2004.08.002.

[33] Y. Lee, Z. C. Feng, Dynamic responses to sinusoidal excitations of beams with frictional joints, Communications in Nonlinear Science and Numerical Simulation 9 (2004) 571–581. doi:10.1016/S1007-5704(03)00060-1.

[34] T. Friis, M. Tarpø, E. I. Katsanos, R. Brincker, Equivalent linear systems of nonlinear systems, Journal of Sound and Vibration 469 (2020). doi:10.1016/j.jsv.2019.115126.

[35] A. Klarbring, A. Mikelić, M. Shillor, Frictional contact problems with normal compliance, International Journal of Engineering Science 26 (1988) 811–832. doi:10.1016/0020-7225(88)90032-8.

[36] A. A. Ferri, A. C. Bindemann, Damping and Vibration of Beams With Various Types of Frictional Support Conditions, Journal of Vibration and Acoustics 114 (1992) 289–296. URL: https://asmedigitalcollection.asme.org/vibrationacoustics/article/114/3/289/454427/Damping-and-Vibration-of-Beams-With-Various-Types. doi:10.1115/1.2930260.

[37] G. P. Wright, J. J. O'Connor, Finite-element analysis of alternating axial loading of an elastic plate pressed between two elastic rectangular blocks with finite friction, International Journal of Engineering Science 9 (1971) 555–570. doi:10.1016/0020-7225(71)90038-3.

[38] H. Ramsey, Analysis of interwire friction in multilayered cables under uniform extension and twisting, International Journal of Mechanical Sciences 32 (1990) 709–716. URL: https://linkinghub.elsevier.com/retrieve/pii/0020740390900117. doi:10.1016/0020-7403(90)90011-7.

[39] L. Frýba, S. Nakagiri, N. Yoshikawa, Stochastic Finite Elements for a Beam on a Random Foundation with Uncertain Damping Under a Moving Force, Journal of Sound and Vibration 163 (1993) 31–45. URL: https://linkinghub.elsevier.com/retrieve/pii/S0022460X83711466. doi:10.1006/jsvi.1993.1146.

[40] A. Cicirello, R. S. Langley, The vibro-acoustic analysis of built-up systems using a hybrid method with parametric and non-parametric uncertainties, Journal of Sound and Vibration 332 (2013) 2165–2178. URL: http://dx.doi.org/10.1016/j.jsv.2012.05.040https://linkinghub.elsevier.com/retrieve/pii/S0022460X12004701. doi:10.1016/j.jsv.2012.05.040.

[41] A. Cherki, G. Plessis, B. Lallemand, T. Tison, P. Level, Fuzzy behavior of mechanical systems with uncertain boundary conditions, Computer Methods in Applied Mechanics and Engineering 189 (2000) 863–873. doi:10.1016/S0045-7825(99)00401-6.

[42] T. G. Ritto, R. Sampaio, E. Cataldo, Timoshenko beam with uncertainty on the boundary conditions, Journal of the Brazilian Society of Mechanical Sciences and Engineering 30 (2009) 295–303. doi:10.1590/s1678-58782008000400005.

[43] S. Li, E. Reynders, K. Maes, G. De Roeck, Vibration-based estimation of axial force for a beam member with uncertain boundary conditions, Journal of Sound and Vibration 332 (2013) 795–806. URL: http://dx.doi.org/10.1016/j.jsv.2012.10.019https://linkinghub.elsevier.com/retrieve/pii/S0022460X12008206. doi:10.1016/j.jsv.2012.10.019.

[44] H. Ahmadian, H. Jalali, F. Pourahmadian, Nonlinear model identification of a frictional contact support, Mechanical Systems and Signal Processing 24 (2010) 2844–2854. URL: http://dx.doi.org/10.1016/j.ymssp.2010.06.007https://linkinghub.elsevier.com/retrieve/pii/S0888327010001998. doi:10.1016/j.ymssp.2010.06.007.

[45] K. Asadi, H. Ahmadian, H. Jalali, Micro/macro-slip damping in beams with frictional contact interface, Journal of Sound and Vibration 331 (2012) 4704–4712. URL: http://dx.doi.org/10.1016/j.jsv.2012.05.026https://linkinghub.elsevier.com/retrieve/pii/S0022460X12004117. doi:10.1016/j.jsv.2012.05.026.

[46] H.-I. Won, J. Chung, Numerical analysis for the stick-slip vibration of a transversely moving beam in contact with a frictional wall, Journal of Sound and Vibration 419 (2018) 42–62. URL: https://doi.org/10.1016/j.jsv.2017.12.037https://linkinghub.elsevier.com/retrieve/pii/S0022460X17308969. doi:10.1016/j.jsv.2017.12.037.

[47] H. Jrad, J. L. Dion, F. Renaud, I. Tawfiq, M. Haddar, Non-linear generalized maxwell model for dynamic characterization of viscoelastic components and parametric identification techniques, in: Proceedings of the ASME Design Engineering Technical Conference, volume 1, 2012, pp. 291–300. doi:10.1115/DETC2012-70264.

[48] M. Tufekci, S. Gunes-Durak, T. Ormanci-Acar, N. Tufekci, Effects of geometry and PVP addition on mechanical behavior of PEI membranes for use in wastewater treatment, Journal of Applied Polymer Science 47073 (2018) 47073. URL: http://doi.wiley.com/10.1002/app.47073. doi:10.1002/app.47073.

[49] D. J. Riddoch, A. Cicirello, D. A. Hills, Response of a mass-spring system subject to Coulomb damping and harmonic base excitation, International Journal of Solids and Structures 193-194 (2020) 527–534. URL: https://doi.org/10.1016/j.ijsolstr.2020.02.037. doi:10.1016/j.ijsolstr.2020.02.037.

[50] L. Marino, A. Cicirello, D. A. Hills, Displacement transmissibility of a Coulomb friction oscillator subject to joined base-wall motion, Nonlinear Dynamics 98 (2019) 2595–2612. URL: http://link.springer.com/10.1007/s11071-019-04983-x. doi:10.1007/s11071-019-04983-x.

[51] L. Marino, A. Cicirello, Experimental investigation of a single-degree-of-freedom system with Coulomb friction, Nonlinear Dynamics 99 (2020) 1781–1799. URL: https://doi.org/10.1007/s11071-019-05443-2. doi:10.1007/s11071-019-05443-2.

[52] L. Marino, A. Cicirello, Multi-degree-of-freedom systems with a Coulomb friction contact: analytical boundaries of motion regimes, Nonlinear Dynamics 104 (2021) 35–63. URL: https://doi.org/10.1007/s11071-021-06278-6https://link.springer.com/10.1007/s11071-021-06278-6. doi:10.1007/s11071-021-06278-6.

[53] H. I. Won, B. Lee, J. Chung, Stick-slip vibration of a cantilever beam subjected to harmonic base excitation, Nonlinear Dynamics 92 (2018) 1815–1828. doi:10.1007/s11071-018-4164-7.

[54] S. Acarer, I. Pir, M. Tüfekci, G. Türkoğlu Demirkol, N. Tüfekci, Manufacturing and Characterisation of Polymeric Membranes for Water Treatment and Numerical Investigation of Mechanics of Nanocomposite Membranes, Polymers 13 (2021). URL: https://www.mdpi.com/2073-4360/13/10/1661. doi:10.3390/polym13101661.

[55] M. Tüfekci, S. G. Durak, I. Pir, T. O. Acar, G. T. Demirkol, N. Tüfekci, Manufacturing, characterisation and mechanical analysis of polyacrylonitrile membranes, Polymers 12 (2020) 1–21. doi:10.3390/polym12102378.

[56] M. Krack, J. Gross, Harmonic Balance for Nonlinear Vibration Problems, 2019.

[57] Y. Sun, J. Yuan, E. Denimal, L. Salles, Nonlinear Modal Analysis of Frictional Ring Damper for Compressor Blisk, Journal of Engineering for Gas Turbines and Power 143 (2021). doi:10.1115/1.4049761.

[58] Y. Sun, J. Yuan, L. Pesaresi, E. Denimal, L. Salles, Parametric Study and Uncertainty Quantification of the Nonlinear Modal Properties of Frictional Dampers, Journal of Vibration and Acoustics 142 (2020). URL: https://doi.org/10.1115/1.4046953https://asmedigitalcollection.asme.org/vibrationacoustics/article/doi/10.1115/1.4046953/1082704/Parametric-Study-and-Uncertainty-Quantification-of. doi:10.1115/1.4046953.

[59] Y. Sun, J. Yuan, L. Pesaresi, L. Salles, Parametric Study and Uncertainty Quantification of the Nonlinear Modal Properties of Frictional Dampers Parametric Study and Uncertainty Quantification of the Nonlinear Modal Properties of Frictional Dampers, Journal of vibration and acoustics (2020).

[60] Y. Sun, J. Yuan, L. Pesaresi, L. Salles, Nonlinear Vibrational Analysis for Integrally Bladed Disk Using Frictional Ring Damper, Journal of Physics: Conference Series 1106 (2018). doi:10.1088/1742-6596/1106/1/012026.

[61] M. Krack, L. A. Bergman, A. F. Vakakis, On the efficacy of friction damping in the presence of nonlinear modal interactions, Journal of Sound and Vibration 370 (2016) 209–220. URL: http://dx.doi.org/10.1016/j.jsv.2016.01.039. doi:10.1016/j.jsv.2016.01.039.

[62] T. M. Cameron, J. H. Griffin, An Alternating frequency/time domain method for calculating the steady-state response of nonlinear dynamic systems, Journal of Applied Mechanics, Transactions ASME 57 (1990) 251. doi:10.1115/1.2888315.

[63] E. L. Allgower, K. Georg, Introduction to numerical continuation methods, volume 45, Springer, Fort Collins, Colorado, 1990. doi:10.1137/1.9780898719154.